

pubs.acs.org/joc Article

Molecular Engineering of Stabilized Silicon-Rosindolizine Shortwave Infrared Fluorophores

William E. Meador, Timothy A. Lewis, Abdul K. Shaik, Kalpani Hirunika Wijesinghe, Boqian Yang, Amala Dass, Nathan I. Hammer, and Jared H. Delcamp*



Cite This: J. Org. Chem. 2024, 89, 2825–2839



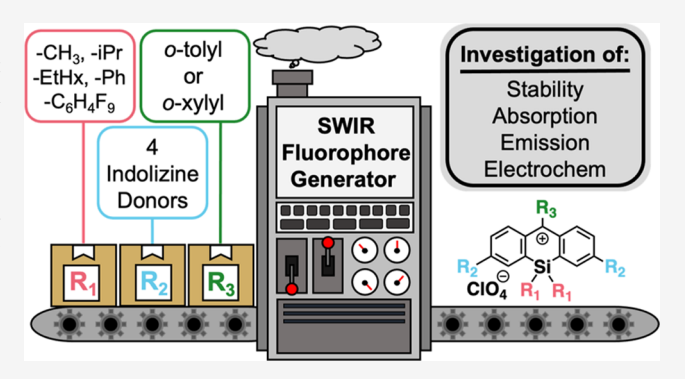
ACCESS I

III Metrics & More

Article Recommendations

Supporting Information

ABSTRACT: Fluorescence-based biological imaging in the shortwave infrared (SWIR, 1000–1700 nm) is an attractive replacement for modern *in vivo* imaging techniques currently employed in both medical and research settings. Xanthene-based fluorophores containing heterocycle donors have recently emerged as a way to access deep SWIR emitting fluorophores. A concern for xanthene-based SWIR fluorophores though is chemical stability toward ambient nucleophiles due to the high electrophilicity of the cationic fluorophore core. Herein, a series of SWIR emitting siliconrosindolizine (SiRos) fluorophores with emission maxima >1300 nm (up to 1550 nm) are synthesized. The SiRos fluorophore photophysical properties and chemical stability toward nucleophiles are examined through systematic derivatization of the silicon-core



alkyl groups, indolizine donor substitution, and the use of *o*-tolyl or *o*-xylyl groups appended to the fluorophore core. The dyes are studied via absorption spectroscopy, steady-state emission spectroscopy, solution-based cyclic voltammetry, time-dependent density functional theory (TD-DFT) computational analysis, X-ray diffraction crystallography, and relative chemical stability over time. Optimal chemical stability is observed via the incorporation of the 2-ethylhexyl silicon substituent and the *o*-xylyl group to protect the core of the fluorophore.

INTRODUCTION

Shortwave infrared (SWIR, 1000-1700 nm) absorbing and emitting organic fluorophores are important materials due to their potential for improving applications such as fluorescence-based biological imaging, $^{1-6}$ hybrid organic photodetectors, $^{7-10}$ and organic light-emitting diodes. $^{11-13}$ Specifically, for fluorescence-based biological imaging, SWIR radiation encounters minimal absorption and scattering when passing through tissues, and the autofluorescence spectrum of tissue diminishes substantially past 1300 nm.^{1,14} These factors generate a biological window for SWIR radiation and provide an unparalleled signal-to-noise ratio for fluorescence imaging. For this reason, SWIR emitting materials are being researched for their potential as fluorescence-based biological imaging agents. Within the past decade, there has been significant research toward small-molecule organic fluorophores emitting past or near 1100 nm with representatives from a variety of fluorophore classes including cyanines, 3,15-21 BODIPYs, squaraines,²⁴ benzothiadiazoles,^{25–27} and xanthenes.^{6,28–32} However, despite intense research into SWIR emitting fluorophores, there remain few small-molecule organic fluorophores reported that emit past 1300 nm. 16,21 Another issue encountered with SWIR emitting fluorophores is chemical stability. As the absorption and emission of a

fluorophore shift to longer wavelengths, the optical energy gap must decrease either by raising the highest occupied molecular orbital (HOMO) or by lowering the lowest unoccupied molecular orbital (LUMO). SWIR fluorophores like xanthenes employ a delocalized cation in the π -system, resulting in low-lying LUMOs and consequent high electrophilicity and instability toward biologically relevant nucleophiles like water, glutathione, and cysteine. While the electrophilicity of these molecules is unavoidable, appropriate synthetic modifications can be made to block electrophilic sites from nucleophilic attack. Thus, dye designs allowing for kinetic persistence of xanthene fluorophores in nucleophile-rich aqueous environments are desirable. 28,31,33 Herein, the photophysical and chemical stability properties of SWIR emitting fluorophores containing a silicon-xanthene core and indolizine donors, termed silicon-rosindolizine (SiRos), are tuned via alteration of the silicon alkyl groups, substitution of the

Received: August 24, 2023 Revised: November 27, 2023 Accepted: January 5, 2024 Published: February 9, 2024





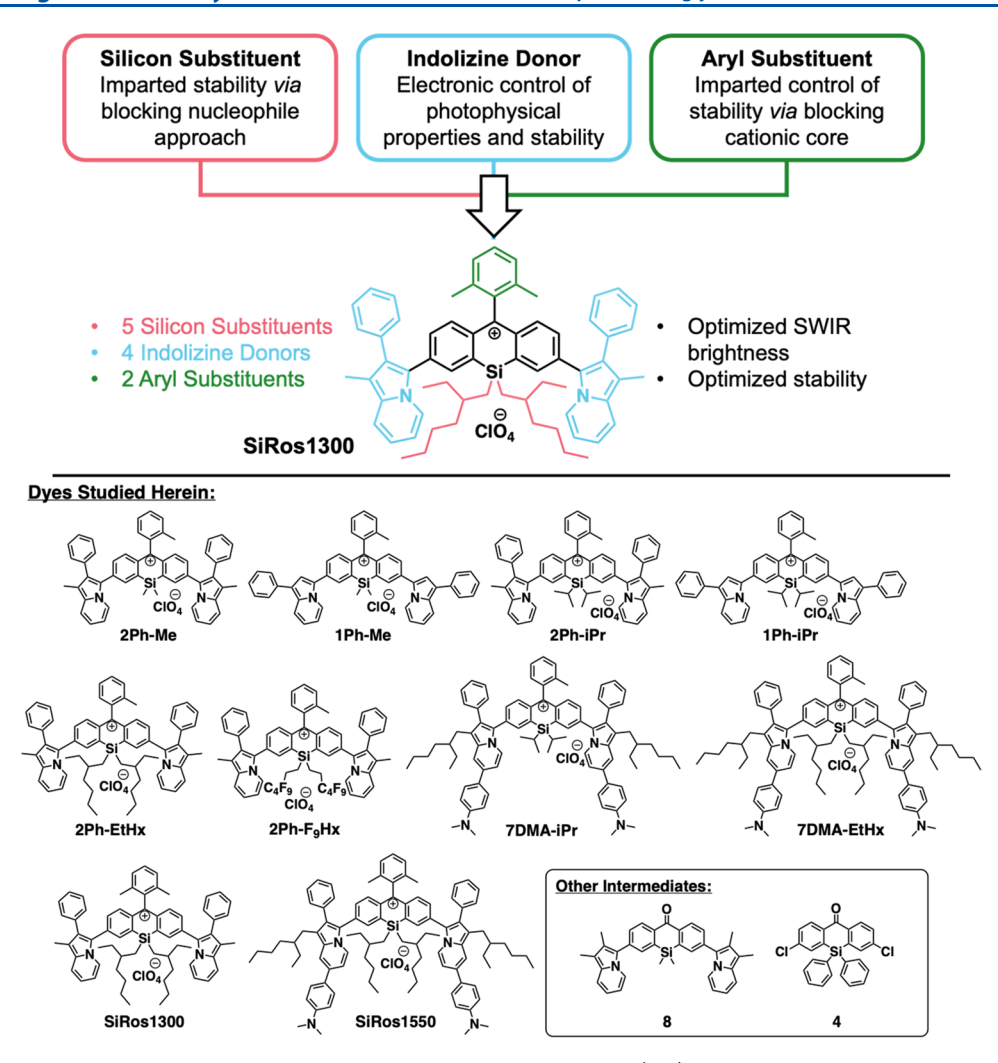
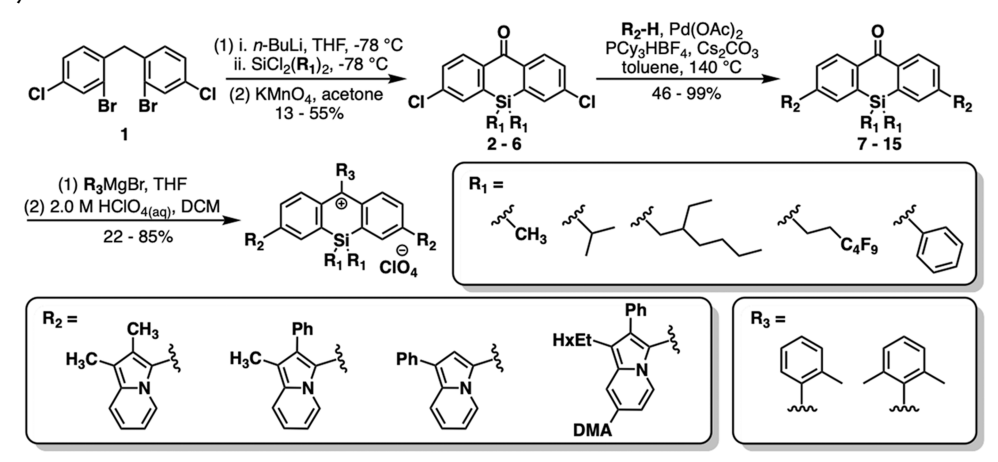


Figure 1. SiRos fluorophore tunable substituents for steric and electronic modulation (top) and the fluorophores made herein (bottom).

Scheme 1. Full Synthetic Route of the SiRos Derivatives



indolizine donors, and modulation of the steric environment imparted by an aryl group appendage at the core of the fluorophore (Figure 1).

■ RESULTS AND DISCUSSION

Synthesis. The SiRos derivatives were synthesized in a manner similar to what was previously described (Scheme 1).³² The route began with double lithium bromide exchange

of 1 (synthesized as previously described),³² followed by reaction with the respective dichlorosilane and oxidation with KMnO₄ to yield **2–6** in yields ranging from 13 to 55%. A variety of dichlorosilanes were investigated as potential substituent introducing groups, including dichlorosilanes bearing two methyls, isopropyls, 2-ethylhexyls, nonafluorohexyls, or phenyls. Further derivatives including dichlorosilanes bearing two trimethylsiloxys, ethoxys, *tert*-butyls, and the cyclic

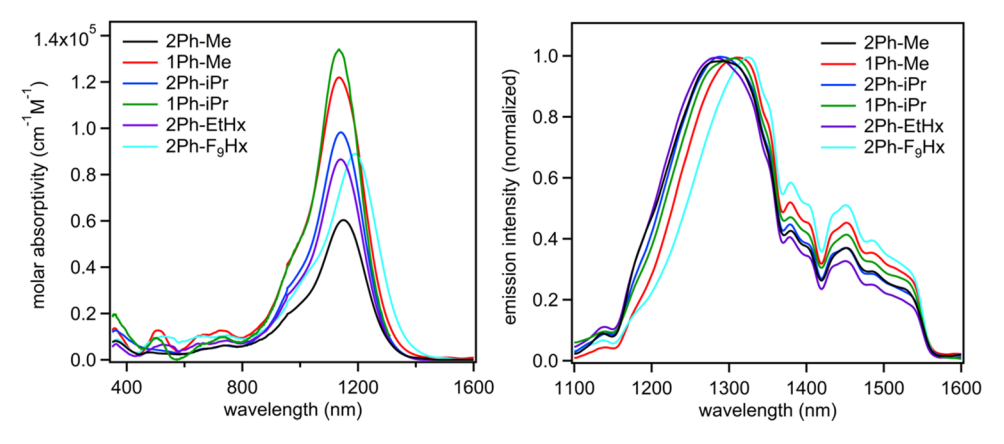


Figure 2. Molar absorptivity of the SiRos dyes containing the 2Ph and 1Ph indolizine donors in DCM (left) and normalized emission spectrum in DCM (right). Note that the dips in the emission spectrum are from solvent reabsorption (see Figure S10).

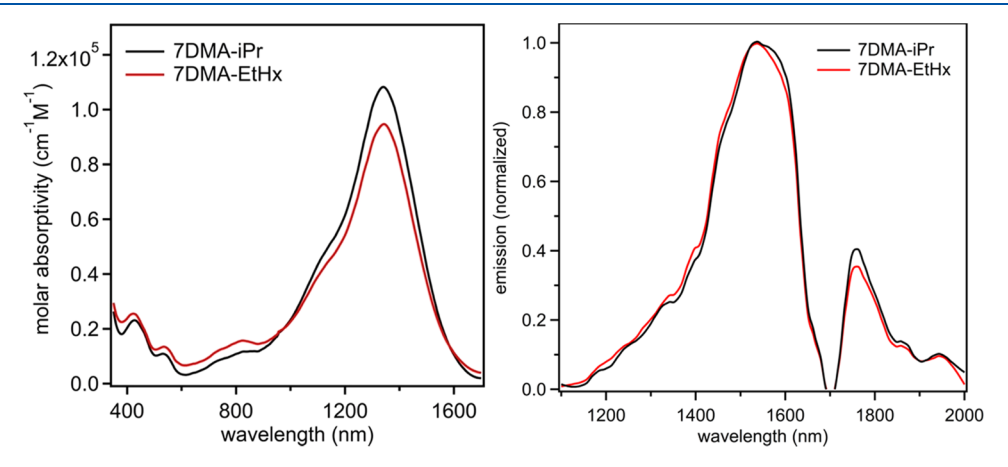


Figure 3. Molar absorptivity of the SiRos dyes containing the 7DMA indolizine donor in DCM (left) and normalized emission spectrum in DCM (right). Note that the dips in the emission spectrum are from solvent reabsorption (see Figure S10).

Table 1. Photophysical and Electrochemical Data of the Dyes in the Specified Solvents^a

dye	λ_{abs} (nm)	λ_{emis} (nm)	Stokes shift (nm eV)	molar abs. $(M^{-1} cm^{-1})$	Φ_{F} (%)	$MB (cm^{-1} M^{-1})$	$E_{(S/S-)}(V)$	$E_{(S+/S)}(V)$
2Ph-Me	1150	1298	148 0.122	63,000	0.0051	3.2	-1.53	-0.46
1Ph-Me	1136	1311	175 0.146	127,000	0.0034	4.3	-1.46	-0.40
2Ph-iPr	1138	1288	150 0.127	103,000	0.0039	4.0	-1.60	-0.46
1Ph-iPr	1132	1304	172 0.144	134,000	0.0045	6.0	-1.56	-0.42
2Ph-EtHx	1141	1280	139 0.118	91,000	0.0049	4.4	-1.64	-0.47
2Ph-F ₉ Hx	1189	1324	135 0.106	92,000	0.0034	3.1	-1.43	-0.37
7DMA-iPr	1338	1550	212 0.127	107,000	0.0027	2.9	-1.64	-0.59
7DMA-EtHx	1339	1544	208 0.125	95,000	0.0032	3.0	-1.65	-0.59
SiRos1300 ^b	1140	1300	160 0.134	115,000	0.0056	6.4	-1.68	-0.45
SiRos1550 ^b	1348	1557	209 0.123	122,000	0.0025	3.1	-1.74	-0.62

^aElectrochemical potentials shown are referenced to the oxidation of ferrocene (Fc⁺/Fc) in DCM with 0.1 M NBu₄PF₆ as a supporting electrolyte. ^bData from ref 32.

silacyclobutane were also investigated but were observed to produce no product from the reaction sequence (Figure S1). The silacyclobutane derivative was observed to form the silylated product from the lithiation reaction but decompose in the following oxidation step. The decomposition pathway is likely due to ring-opening via carbanion formation as has been seen previously for silacyclobutanes^{34,35} due to the distortional energy of the four-membered ring and the propensity to open in the presence of oxyanions. With bridges 2–6 in hand, CH-activation cross-coupling reactions could be performed to install the respective indolizine donors (synthesized as

previously described^{18,36,37}) to obtain 7–15 in good yields spanning from 46 to 99%. A Grignard reaction with otolylmagnesium bromide or o-xylylmagnesium bromide followed by acid workup with aqueous perchloric acid afforded the final dyes in yields ranging from 22 to 85%. The isolated yields are likely deflated for some of the derivatives due to instability of the fluorophores, specifically those bearing the otolyl group, on silica gel during chromatographic separation. The derivative containing 1,2-dimethylindolizine was observed to form the final dye during the acid workup but decomposed rapidly during isolation and was not pursued further. The rest

of the indolizines formed stable, isolable materials that were subsequently studied for their photophysical and electrochemical properties.

Photophysical and Electrochemical Data. Absorption spectroscopy was conducted in dichloromethane (DCM) with the SiRos derivatives to observe how the structural modifications influence the absorption wavelength (λ_{abs}) and molar absorptivity (ε) of the materials (Figures 2 and 3, Table 1). SiRos derivatives containing the 2Ph indolizine donor exhibited modestly longer wavelength λ_{abs} values (1138–1189 nm) than derivatives containing the 1Ph indolizine donor (1132–1136 nm, Figure 2). Another observation between the 1Ph and 2Ph indolizine SiRos derivatives is the difference in the higher energy absorption features of the dyes. Derivatives with 2Ph have a low intensity and a relatively featureless higher energy portion of their absorption spectrum, while derivatives employing 1Ph have a distinct transition at ~500 nm. This is consistent with computation (see the discussion below) wherein the 1Ph derivative has a vertical transition with a notable oscillator strength (>0.1) at 517 nm, while the 2Ph derivative does not exhibit any high-energy vertical transitions with a notable oscillator strength (Table S2). The 2Ph-F₉Hx had the longest wavelength λ_{abs} of the 2Ph derivatives by nearly 40 nm (the other 2Ph derivatives were grouped within 12 nm of one another) with a λ_{abs} of 1189 nm. This is likely due to the perfluorinated hexyl chains lowering the LUMO, but not the HOMO, and thus the energy of the electronic transition (see electrochemical discussion below for reasoning). The 2Ph-**EtHx** and **SiRos1300** dyes are observed to have λ_{abs} within 1 nm of one another (1141 and 1140 nm, respectively), suggesting that switching between the o-tolyl and o-xylyl groups at the central position of the core has very little effect on the optical energy gap of the dyes. As observed previously for SiRos1550, the 7DMA-iPr and 7DMA-EtHx derivatives exhibit lower energy $\lambda_{\rm abs}$ (1336 and 1338 nm, respectively) than the 1Ph or 2Ph derivatives due to the extended π conjugation and increased donation strength of the additional N,N-dimethylaniline (DMA) donor at the 7-position of the indolizine (Figure 3, left). Both 7DMA-iPr and 7DMA-EtHx are slightly blue-shifted (~10 nm) compared to SiRos1550, but in this spectral region, the energy difference is minuscule at <0.01 eV. The absorption of the SiRos dyes was also collected in chloroform (CHCl₃), acetonitrile (MeCN), and chlorobenzene (CB, Figures S2–S9 and Table S1). In CHCl₃, λ_{abs} is comparable to that in DCM with 3-12 nm variation for the 2Ph derivatives, 0-2 nm variation for the 1Ph derivatives, and a 16-18 nm variation with the 7DMA derivatives. In MeCN, $\lambda_{\rm abs}$ is consistently blue-shifted (34–64 nm) and broadened compared to λ_{abs} in DCM, indicating that more polar solvents widen the optical gap of these materials. In CB, λ_{abs} of the dyes is inconsistently shifted overall but shows a trend based on the indolizine donor employed. The 2Ph derivatives exhibit an 18-26 nm bathochromic shift with respect to DCM, while 2Ph-F_oHx is an outlier with a 12 nm blue shift in CB with respect to DCM. The 1Ph derivatives exhibit 4 and 7 nm blue shifts compared to DCM for 1Ph-Me and 1Ph-iPr, respectively. Lastly, the 7DMA derivatives exhibit sizable 42 and 43 nm bathochromic shifts in CB with respect to DCM for 7DMA-iPr and 7DMA-EtHx, respectively.

The molar absorptivity (ε) of the SiRos derivatives was also observed to vary for the 1Ph and 2Ph derivatives (Figure 2 and Table 1). 1Ph derivatives were observed to have a distinctly larger ε (127,000–134,000 M⁻¹ cm⁻¹) than the 2Ph

derivatives (63,000-115,000 M⁻¹ cm⁻¹). This is presumably due to the increased planarity of the 1Ph derivatives that results from the lack of steric repulsion between hydrogens on the phenyl ring at the 2-position of the indolizine and the chromophore core, resulting in better orbital overlap. The 7DMA derivatives were observed to have a slightly higher ε than their respective 2Ph comparisons, with 7DMA-iPr exhibiting a ε of 107,000 M⁻¹ cm⁻¹ and 7DMA-EtHx exhibiting a ε of 95,000 M⁻¹ cm⁻¹ (Figure 3 and Table 1). All of the dyes demonstrated consistently lower ε in the other three solvents (CHCl₃, MeCN, and CB) utilized in this study relative to DCM (Figures S2-S9 and Table S1). The 7DMA derivatives exhibit a smaller relative overall decrease in ε in the other three solvents compared to the 1Ph and 2Ph derivatives, and the 2Ph-F₉Hx was observed to have the greatest relative decrease in ε in the other three solvents compared to DCM (Table S1).

Fluorescence emission spectroscopy was conducted on the SiRos derivatives to probe the effects of each structural modification on the emission wavelength maxima ($\lambda_{\rm emis}$), Stokes shift (energy difference between λ_{abs} and λ_{emis}), fluorescence quantum yield (Φ_F) , and molecular brightness (MB, product of ε and $\Phi_{\rm F}$) of the fluorophores (Figures 2, 3, and S10-S18, Table 1). The 2Ph derivatives were observed to emit at shorter wavelengths than the 1Ph derivatives, except for 2Ph-F₉Hx. Since the 2Ph derivatives were also observed to absorb at longer wavelengths, this resulted in a consistently smaller Stokes shift (0.11-0.13 eV) compared to the 1Ph derivatives (0.14-0.15 eV). This observation is somewhat surprising given that the Stokes shift is reflective of the molecular reorganization between the ground- and excitedstate geometries of a fluorophore. This suggests that the excited-state geometry has a greater dihedral angle than the ground state for the indolizine donors and the silicon-xanthene core since the 1Ph donor has a much smaller dihedral angle about the core (28.6°) than the 2Ph donor (35.3°) in the ground state. The Φ_F of the fluorophores has no apparent trend based on the silicon substituent or indolizine donor for the 1Ph and 2Ph derivatives with the following order: 2Ph- $F_0Hx = 1Ph-Me < 2Ph-iPr < 1Ph-iPr < 2Ph-EtHx < 2Ph-Me$. While **2Ph-Me** exhibits the highest Φ_F , it also has the lowest ε of the series (63,000 M⁻¹ cm⁻¹), which puts it toward the bottom for MB, which considers both absorptivity and emissivity. For the xylyl groups, SiRos1300 has a greater Φ_F than 2Ph-EtHx, but 7DMA-EtHx has a greater $\Phi_{\scriptscriptstyle F}$ than SiRos1550, indicating there is no apparent trend between the aryl group used and Φ_F . The MB of the fluorophores is as follows: $2Ph-F_0Hx < 2Ph-Me < 2Ph-iPr < 2Ph-EtHx < 1Ph-$ Me < 1Ph-iPr. Even though the 1Ph donors have comparable $\Phi_{\rm F}$ to the 2Ph derivatives, the MB values exhibit the importance of the 1Ph derivatives having $\sim 30\%$ higher ε than the highest 2Ph derivative, which results in a greater MB. While the Φ_F values reported herein are on par with what would be expected for fluorophores in this region, 6,16,28 the actual Φ_F values are likely slightly higher than the reported values due to solvent reabsorption of emitted light (Figure S10, seen as the dips in the emission spectra) and the InGaAs detector efficiency drop off at 1550 nm since a previous work shows the emission of these fluorophore tails out to ~1800 nm. 32 Accounting for these losses, the Φ_F is likely ~10–20% greater than the values reported herein based on best estimates. The absorption and emission spectra of the fluorophores are also observed to mirror each other, indicating

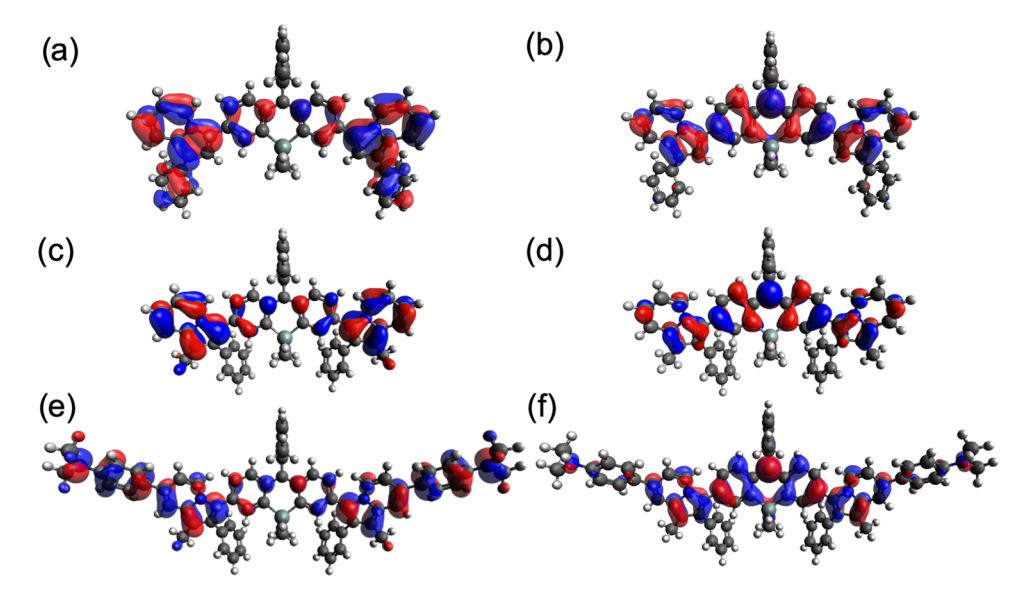


Figure 4. Frontier molecular orbitals of the SiRos derivatives with the Me core and their respective indolizine donors computed at the B3LYP/6-311g(d,p) level of theory using DCM as an implicit solvent. (a) HOMO and (b) LUMO of the 1Ph derivative, (c) HOMO and (d) LUMO of the 2Ph derivative, and (e) HOMO and (f) LUMO of the 7DMA derivative.

that the shoulder feature observed in the absorption spectra is vibronic in nature (Figures S11–S18).

Cyclic voltammetry (CV) was conducted for the SiRos derivatives to determine the ground-state electrochemical oxidation $(E_{(S+/S)})$ and reduction $(E_{(S/S-)})$ potentials of the materials (Figures S19-S26, Table 1). The potentials can be used to assess ambient stability as well as suitability for these materials in optoelectronic device applications. The CVs were taken in DCM with a 0.1 M NBu₄PF₆ electrolyte and are referenced to Fc⁺/Fc at 0.00 V. The $E_{(S+/S)}$ values of the fluorophores were tuned by the indolizine donor employed in the structure, with 2Ph derivatives having $E_{(S+/S)}$ centered around -0.46 V (-0.45 to -0.47 V), 1Ph derivatives having $E_{\rm (S+/S)}$ centered around -0.41 V (-0.40 to -0.42 V), and 7DMA derivatives having $E_{(S+/S)}$ centered around -0.60 V (-0.59 to -0.62 V). This indicates that the 7DMA donor is the most electron-rich donor of the series, followed by the 2Ph donor, which is observed to be more electron-rich than the 1Ph donor. The lone outlier from this trend is the 2Ph-F₉Hx, which has an $E_{(S+/S)}$ of -0.37 V. This value is shifted ~ 0.09 V toward more positive potentials compared to the other 2Ph derivatives. The observation of the 2Ph-F_oHx being an outlier is consistent with the absorption and emission spectroscopy and is hypothesized to be due to the perfluorinated hexyl chains influencing the optical and electrochemical properties of the dye. The $E_{(\mathrm{S/S-})}$ values of the tolyl containing derivatives are only quasi-reversible. The $E_{(S/S-)}$ values of the 1Ph derivatives are shifted toward more positive potentials relative to the respective 2Ph derivative; however, the grouping of the potentials is not as tight as seen for the $E_{(S+/S)}$ values, with $E_{\rm (S/S-)}$ from -1.46 to -1.56 V for the 1Ph derivatives and -1.53 to -1.64 V for the 2Ph derivatives. **2Ph-F₉Hx** also has the most positively shifted $E_{(S/S-)}$ at -1.43 V, coinciding with what was observed for the oxidation potentials. 7DMA-iPr and 7DMA-EtHx exhibit more positively shifted $E_{(S/S-)}$ than SiRos1550. The observation that the $E_{(S/S-)}$ values of the tolyl derivatives are quasi-reversible while that of the xylyl derivatives are observed to be reversible indicates rapid chemical reactivity at the core following reduction. A good

example for analysis is **2Ph-EtHx** and **SiRos1300**, where the only structural difference is the presence of the additional *ortho*-methyl of the xylyl group offering steric protection for both sides of the core. This implies that the chemical reaction occurs at the central core of the **2Ph-EtHx** dye following reduction and does not allow for the subsequent removal of the electron from the reduced dye due to transformation to a new chemical species. This reaction is kinetically inaccessible for **SiRos1300** due to the steric protection of the reduced core, which allows for the removal of the electron during the return sweep. Computational analysis also indicates reduction occurring at the core of the fluorophore with the LUMO heavily localized on the core (see computational discussion below) and a particularly large coefficient at the central position of the core.

Computational Data. Time-dependent density functional theory (TD-DFT) calculations were conducted for the SiRos derivatives at the B3LYP/6-311g(d,p)38-40 level of theory using DCM as an implicit solvent with Gaussian16 software⁴ (Figure 4 and Table S2). Analysis of the HOMO and LUMO distribution obtained from DFT demonstrates the HOMO is primarily localized on the indolizine donors with lesser distribution on the core. The LUMO is distributed more evenly across the entire molecule with particularly large coefficients on the core. For the 1Ph derivative, the HOMO extends onto the phenyl group of the indolizine donor, whereas for the 2Ph derivative, there is no significant HOMO distribution on the phenyl group of the indolizine donor. This is likely due to the lack of the HOMO coefficient at the 2carbon of the indolizine donor compared to the particularly large HOMO coefficient at the 1-carbon of the indolizine donor. For the 7DMA derivative, the HOMO is observed to extend onto the DMA donor, while the LUMO has modest distribution on the DMA group. This observation is consistent with the electrochemical measurements in which the DMA group shifts $E_{(S+/S)}$ to more negative energies (0.12 V for 2Ph-EtHx and 7DMA-EtHx), indicating an increase in the energy of the HOMO orbital, while nearly leaving the $E_{(S/S-)}$ energy unperturbed (0.01 V for 2Ph-EtHx and 7DMA-EtHx).

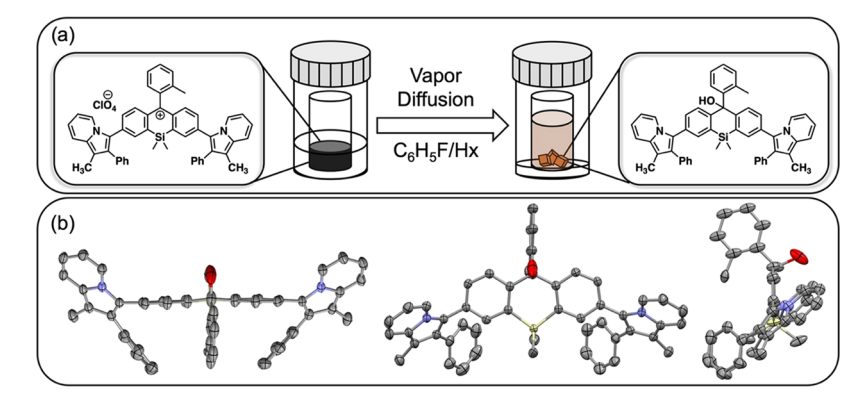


Figure 5. Crystallographic data demonstrating electrophilicity at the central atom of the silicon-xanthene core. (a) Graphical representation of the chemical transformation from the starting **2Ph-Me** dye to the hydroxyl added, crystallized product. (b) Crystal structure of **2Ph-Me**—OH from different perspectives. The structures shown are thermal ellipsoid plots at 50% probability. The crystals were grown via vapor diffusion of hexanes into a solution of **2Ph-Me** in fluorobenzene over a period of 4 days.

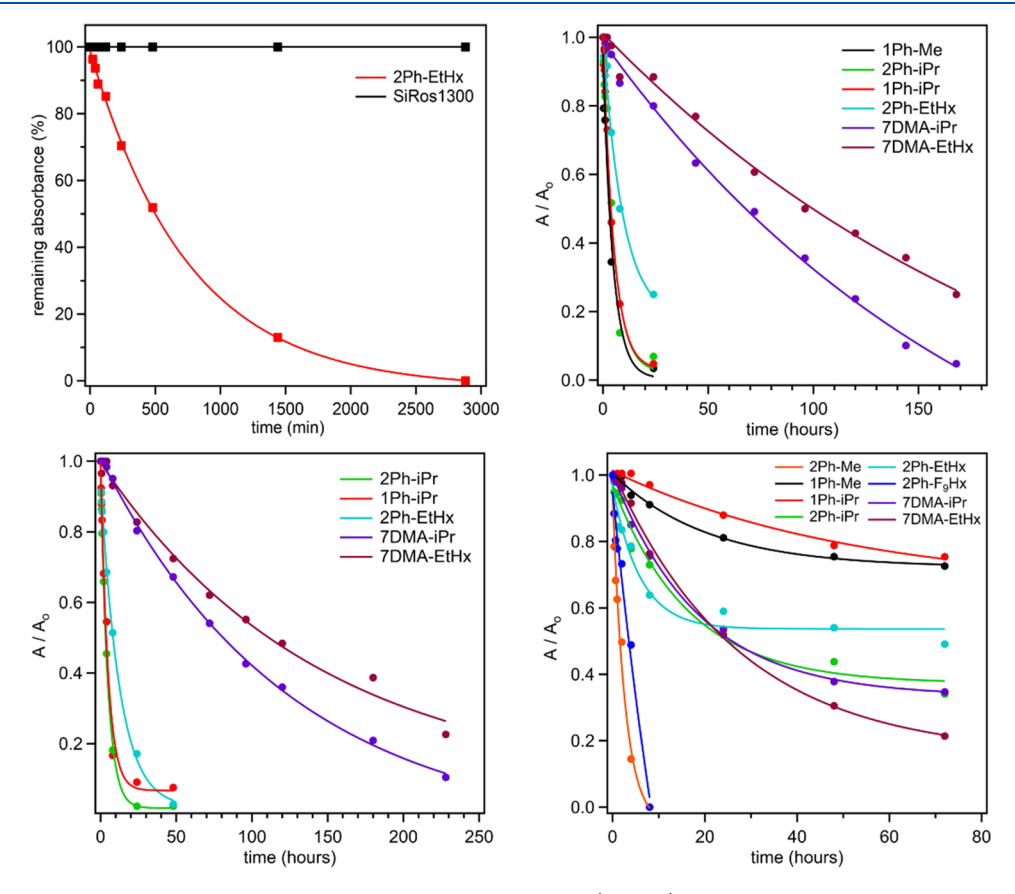


Figure 6. Stability of 2Ph-EtHx and SiRos1300 in 99% MeCN/1% H_2O solution (top left), stability of SiRos dyes in 1% H_2O /MeCN (top right), 0.5 M AcOH (bottom left), and 0.5 M trifluoroacetic acid (TFA, bottom right). Note that some dyes are not included in all of the graphs as they decomposed too rapidly to observe the decay kinetics.

Vertical transitions for **2Ph-Me** and **1Ph-Me** are observed to have a negligible difference (0.06 eV), which coincides with the very similar λ_{abs} in DCM observed experimentally. In DCM, the **2Ph-Me** derivative exhibits a lower energy λ_{abs} than the **1Ph-Me** derivative (1150 and 1136 nm, respectively); however, TD-DFT calculations predict a lower energy vertical transition for the **1Ph-Me** derivative than the **2Ph-Me** derivative (846 and 811 nm, respectively). In both cases, the λ_{abs} and vertical transition energies are very close in energy though (0.01 and 0.06 eV, respectively) with negligible differences. TD-DFT predicts a higher oscillator strength for

1Ph-Me (1.47) than **2Ph-Me** (1.27), which is consistent with experimental observations where the 1Ph derivatives have a larger ε than the 2Ph derivatives. A further increase in oscillator strength is observed upon addition of the 7DMA donor; however, this is not correlated experimentally with ε as the 7DMA derivatives have a lower ε than the 1Ph derivatives and only a slightly higher molar absorptivity to the 2Ph derivatives. Both the 1Ph and 7DMA derivatives are also observed to have higher energy vertical transitions via TD-DFT, which is apparent in their DCM absorption spectra (Figures 2 and 3, Table S2). For the 1Ph derivatives, this

higher energy transition is observed to occur at 517 nm with an oscillator strength of 0.23 and originates from HOMO-2, which is primarily situated on the phenyl group located at the 1-position of the donor, to the LUMO orbital (Table S2 and Figure S27). For the 7DMA derivatives, there are two higher energy transitions. The first one is observed to occur at 678 nm with an oscillator strength of 0.21 and originates from the HOMO-2, which is primarily situated on the DMA group located at the 7-position of the donor, to the LUMO orbital (Figure S27). The second vertical transition is observed to occur at 439 nm with an oscillator strength of 0.20 and originates from the HOMO orbital to the LUMO+1 orbital, which is spread across the core and indolizines of the chromophore (Figure S27).

X-ray Diffraction Crystallography Data. Single-crystal X-ray diffraction (XRD) studies were pursued to better understand the orientation and geometry of the molecular structure. The 2Ph-Me derivative was selected for comparison to PhRosIndz as well as other indolizine-donor-based fluorophore derivatives previously studied through XRD. 28,37,42 Several techniques with a range of solvent combinations were tried including vapor diffusion, slow evaporation, and hot/cold recrystallization. Of these techniques, only one successful batch of crystals was grown via the vapor diffusion of hexanes into a saturated solution of 2Ph-Me in fluorobenzene. XRD analysis of the obtained crystals did not yield the expected 2Ph-Me fluorophore though and instead yielded the hydroxylated product, 2Ph-Me-OH (Figures 6a and S28-S30, Tables S3-S10). This finding was somewhat surprising as the pure dye was introduced to the solution, and this indicates that residual water present in the experiment was sufficient to add to the core of the fluorophore and result in crystallization of the hydroxylated material. The obtained structure once again demonstrates the electrophilicity of the central position on the xanthene core and conveniently shows that hydroxylation occurs opposite the sterically blocking methyl of the o-tolyl ring as one might expect (Figure 5b). Another interesting observation is the orientation of the indolizine donors about the core, where the phenyl ring at the 2-position of the indolizine is oriented down and away from the central aryl ring. In the crystal structure of PhRosIndz, the same phenyl ring is observed to point upward toward the central aryl ring of the fluorophore. The difference in orientation could be due to the PhRosIndz being the cationic, final dye, while 2Ph-Me-OH is a neutral derivative, or that the orientations are both close in energy. XRD analysis further implicates the central core of the chromophore as the most prevalent electrophilic site and demonstrates the importance of pursuing steric blocking groups on both sides of the central aryl ring to impart kinetic persistence to the fluorophore class.

Fluorophore Stability. Stability studies were conducted in three different solvent systems: 99% MeCN/1% H_2O , 99% MeCN/1% H_2O with 0.5 M acetic acid (AcOH), and 99% MeCN/1% H_2O with 0.5 M trifluoroacetic acid (TFA) as done previously for a comparable fluorophore scaffold (Figure 6, Table 2).³¹ The half-life of each dye was calculated by taking the remaining λ_{max} absorbance at a given time over the initial λ_{max} absorbance to get the percent absorbance remaining over a period of time. Absorbance measurements were taken via NIR absorption spectroscopy at time points spanning up to a two-week period. In the 99% MeCN/1% H_2O solutions, the stability trend of the silicon R-group was observed to be Me = F_9Hx < iPr < EtHx, where **2Ph-Me** and **2Ph-F_9Hx**

Table 2. Half-Life in Hours of the SiRos Dyes in the Respective MeCN Solutions

dye	H_2O^a	AcOH ^b	TFA^c
2Ph-Me			2
1Ph-Me	3		92
2Ph-iPr	4	3	27
1Ph-iPr	4	3	105
2Ph-EtHx	8	8	66
2Ph-F ₉ Hx			3
7DMA-iPr	58	82	27
7DMA-EtHx	83	107	25
SiRos1300	>840	>840	>840
SiRos1550	>840	>840	229

 a 99% MeCN/1% H₂O. b 99% MeCN/1% H₂O with 0.5 M HOAc. c 99% MeCN/1% H₂O with 0.5 M TFA.

decomposed almost instantaneously, and EtHx survived the longest, regardless of donor. The stability trend regarding the indolizine donors was observed to be 2Ph < 1Ph ≪ 7DMA, with the 1Ph being slightly more stable than the 2Ph, and the 7DMA having an order of magnitude longer half-life than either of the other two donors. The dyes employing xylyl groups in place of tolyl groups at the central carbon all lasted a full two-week period with minimal loss in absorbance. Stability was comparable in the plain water systems and the acetic acid systems, with the 7DMA dyes once again showing high longevity relative to the other dyes examined. In TFA systems, however, the 7DMA dyes decreased substantially in stability, with all other tolyl-based dyes showing a significant increase in half-life compared to the other two solvent systems. The decrease in stability of the 7DMA dyes is likely due to protonation of the 7DMA groups, as indicated by a blue shift in their absorbance from \sim 1340 to \sim 1150 nm, which increases the electrophilicity of the fluorophores by withdrawing electron density from the π -system and thus lowering their overall stability. The 1Ph and 2Ph dyes do not have the auxiliary aryl amine donors to protonate and do not suffer from the same increase in electrophilicity in the presence of TFA. Instead, their stability increases as the H₂O in solution is shifted to H_3O^+ due to the low p K_3 of TFA, thus lowering the rate of nucleophilic attack. Interestingly, the 1Ph-Me and 1PhiPr dyes, which decayed relatively quickly in both water and acetic acid solutions, were observed to be the most stable dyes in the TFA-containing solutions, with half-lives of 92 and 105 h, respectively. Across all three solvent systems, the xylyl-based dyes (SiRos1300 and SiRos1550) possessed markedly elevated stability compared to the tolyl-based dyes, with only SiRos1550 in trifluoroacetic acid demonstrating a measurable half-life of less than 2 weeks. This is demonstrated when comparing 2Ph-EtHx and SiRos1300, where 2Ph-EtHx completely decays within a day's time, while SiRos1300 demonstrates no loss in absorption (Figure 6). Overall, use of the bulky EtHx silicon substituents and xylyl group at the core of the fluorophore appears to result in universally higher stability in all conditions tested, which indicates these functionalities are valuable for in vivo imaging. The stability trend for the indolizine donors however is conditiondependent, wherein the 7DMA indolizine donors exhibit greater stability in neutral to mildly acidic conditions, and the 1Ph indolizine donors exhibit greater stability in strongly acidic conditions.

CONCLUSIONS

There is currently a need for small-molecule organic fluorophores that emit in the SWIR due to their plethora of applications in fluorescence-based biological imaging, hybrid organic photodetectors, and organic light-emitting diodes. While there is an abundance of fluorophores with λ_{emis} wavelengths <1300 nm, there are few with $\lambda_{\rm emis}$ wavelengths >1300 nm. Xanthene core-based fluorophores have recently stood out as an attractive option to access SWIR emitting fluorophores, with multiple examples emitting near or past 1100 nm and one exhibiting a $\lambda_{\rm emis}$ of 1700 nm. ³² However, xanthene fluorophores often exhibit high electrophilicity at the central carbon of the fluorophore core and consequent chemical instability toward nucleophiles like water, limiting their use in biological imaging. Herein, a series of SWIR emitting indolizine donor-based silicon-xanthene fluorophores were synthesized, and their photophysical properties and chemical stability were optimized. The fluorophores exhibit λ_{abs} near ~1150 nm (for 1Ph and 2Ph indolizing donors) and ~1350 nm (for 7DMA indolizing donors) and λ_{emis} near ~1300 and ~1550 nm, respectively. $\Phi_{\rm E}$ ranged from 0.0025 to 0.0056%. The core of the fluorophore was implicated as the most probable electrophilic site as observed via XRD crystallography of the hydroxylated product, 2Ph-Me-OH. The 2-ethylhexyl silicon substituent proved to be the most effective substituent in slowing decomposition, providing modest improvement in the half-life of the fluorophores in aqueous environments, and the o-xylyl groups demonstrated a substantial improvement in stability relative to the o-tolyl group, with SiRos1300 exhibiting little to no absorption loss by the time structurally similar **2Ph-EtHx** completely decayed. The 7DMA indolizine was observed to be the most stable in neutral to mildly acidic conditions, while the 1Ph indolizine was observed to be the most stable under highly acidic conditions. Overall, this work illustrates a modular way to optimize SWIR fluorophore molecular brightness and chemical stability, factors that are integral in designing future SWIR fluorophores.

■ EXPERIMENTAL SECTION

General Information. Reagents and solvents used in this study were purchased from 1PlusChem, Gelest, Ambeed, TCI, Sigma-Aldrich, Acros Organics, and Thermo Fischer Scientific and were used as received without further purification. Thin-layer chromatography (TLC) was conducted with Sorbtech Silica XHL TLC Plates (Support: glass backed; thickness: 250 μ m) and visualized with a UV lamp. Flash column chromatography was performed using a Teledyne CombiFlash Rf + system. The silica gel cartridges were purchased from Luknova SuperSep (FC003012, 50 μm). ¹H and $^{\hat{1}3}C\{^{1}H\}$ NMR spectra were recorded on a Bruker Ascend-300 (300 MHz) and a Bruker Ascend-400 (400 MHz) spectrometer using deuterated solvents. I values are expressed in Hz, and chemical shifts are in ppm using residual solvent as an internal standard (CDCl₃ at 7.26 ppm, CD_2Cl_2 at 5.32 ppm, and $(CD_3)_2CO$ at 2.05 ppm). Singlet (s), doublet (d), doublet of doublets (dd), triplet (t), multiplet (m), multiple signals (ms), broad (br), and apparent (ap) are designated as ¹H NMR multiplicity patterns. High-resolution mass spectrometry (HRMS) spectra were obtained with a quadrupole time-of-flight (QTOF) HRMS utilizing nanospray ionization. The mass analyzer was set to the 200-2000 Da range. Infrared spectra were recorded with an Agilent Cary 660 attenuated total reflection-Fourier transform infrared (ATR-FTIR) spectrometer. All fluorescence spectra were conducted with a dye concentration of 1×10^{-5} M. The fluorescence emission spectra and fluorescence quantum yield ($\Phi_{\rm E}$, referenced to IR-1061 at 0.32% in DCM)⁴³ of the 1Ph and 2Ph derivatives were

recorded using a HORIBA QuantaMaster 8075–21 spectrofluorometer with xenon lamp excitation and a liquid nitrogen-cooled InGaAs solid-state detector. Φ_{F} was calculated using the following equation

$$\Phi_{\text{sample}} = \Phi_{\text{standard}} \times \frac{E_{\text{sample}}}{E_{\text{standard}}} \times \frac{A_{\text{standard}}}{A_{\text{sample}}} \times \frac{\eta_{\text{sample}}^2}{\eta_{\text{standard}}^2}$$
(1)

where E is the integrated emission count, A is 1×10^{-A} with the superscript A being the absorbance at the excitation wavelength, η is the refractive index of the solvent used, and Φ denotes the fluorescent quantum yield. The fluorescence emission spectra of the 7DMA derivatives were acquired with a HORIBA Fluorolog-QM, the fourth generation of the Fluorolog spectrofluorometer. A 980 nm DPSS (diode pumped solid state, 2W) laser was used as the excitation source and was mounted to the front panel of the Fluorolog-QM's sample tray. A HORIBA LN-cooled DSS InAs detector was used to detect the emission through a monochromator (350 mm focal length) with a ruled diffraction grating (600 grooves/mm, blazed at 1.25 μ m), a scanning increment of 2 nm, and an emission bandpass of 30 nm. To increase the detector's sensitivity, a lock-in amplifier with the LNcooled InAs detector was used. A TTL output signal (27 Hz) from the chopper control was used as the reference signal to the lock-inamplifier control and as the trigger signal to the laser control to electrically chop the 980 nm DPSS laser. The time constant of the lock-in amplifier was set to 100 ms, and the detector integration time was 0.3 s. $\Phi_{\rm E}$ values of 7DMA derivatives were referenced to the value of 0.0056% for SiRos1300 in DCM.³² The recorded emission spectra were all smoothed with a LOESS function. All of the absorption profiles were recorded on a Cary 5000 UV-vis-NIR spectrophotometer set to the double-beam mode with all dyes at a concentration of 1×10^{-5} M. Cyclic voltammetry curves were measured with a C-H Instruments electrochemical analyzer (model CHI602E). All measurements were conducted under an argon atmosphere (~0.5 mL of excess DCM was added along with the electrolyte solution, followed by bubbling of solution with argon until the volume decreased to the original volume of just the electrolyte solution) at room temperature and taken using a platinum counter electrode (flame cleaned before each measurement), a Ag pseudo-reference electrode (cleaned with fine grit sandpaper and a Kimtech wipe before each measurement), and glassy carbon disc working electrode (surface area of 7.07 mm², polished with 0.3 μ m MicroPolish powder purchased from CH Instruments and ethanol over a microcloth polishing pad prior to each measurement, following previously reported polishing techniques).⁴⁴ The analyte concentration was 1 \times 10⁻⁴ M, and the electrolyte solution used was 0.1 M Bu₄NPF₆ in DCM. Ferrocene was used as the reference standard taken as 0.00 V, and oxidation and reduction potentials of the materials are reported versus Fc⁺/Fc in DCM. For all experiments, the scan rate was 100 mV/s, the initial scan direction was positive, and the voltammograms are plotted in polarographic convention. The initial potential of each experiment was approximately the midpoint between the oxidation and reduction peaks. For computation, all of the molecules were first drawn in ChemDraw (20.0.0.41) and saved as MDL Molfile. The geometries of those molecules were then optimized with the MMFF94 force field using Avogadro (1.2.0). Dihedral angles of acyclic single bonds were manually set between 0 and 90° to avoid local minima conformations. Then, sequential geometry optimizations were performed by DFT using Gaussian16⁴ with the B3LYP4 functional and the following basis sets: first 3-21G, then 6-31G(d,p), 47,48 and finally $6-311G(d,p)^{38}$ with a dichloromethane polarizable continuum model. $^{49-51}$ After having the optimized geometries, TD-DFT was performed with the B3LYP functional and the 6-311G(d,p) basis set to compute the vertical transition energies and oscillator strengths. The crystal of 2Ph-Me-OH was grown by dissolving approximately 10 mg of 2Ph-Me in 1.0 mL of fluorobenzene and syringe filtering the solution (0.45 μ m) into a small vial. The small vial was then placed in a larger vial containing hexanes, and the larger vial was sealed and placed in the dark. The crystallization was allowed to occur over several days as the hexane

vapors diffused into the fluorobenzene solution containing 2Ph-Me. After 4 days, examination of the vial revealed that the solution color had changed from black to orange and that there were small yellow crystals in the vial that were observed to be 2Ph-Me-OH upon XRD analysis. See the Supporting Information for XRD experimental details. For the stability studies, a stock solution of each dye was made in DCM at 3×10^{-4} M. The necessary amount of the dye solution (100 μ L) to obtain 3.0 mL of a 1 × 10⁻⁵ M solution was then added to a vial, and the solvent was removed under vacuum-drying. 3.0 mL of MeCN solution containing either 1% H2O, 1% H2O, and 0.5 M AcOH, or 1% H₂O and 0.5 M TFA was then added to the vial to dissolve the dye, transferred to a cuvette, and placed in an OceanInsight FlameNIR+ spectrometer equipped with an HL-2000-HP light source to obtain the initial maximum absorbance at 1×10^{-5} M. The solutions were then stored under ambient conditions, and the change in the absorbance maximum was measured at regular time points to determine the stability of the dyes. All MeCN used was freshly distilled over CaH2, and all DCM used was obtained via a solvent transfer system to minimize additional water content. For crystallography, the selected crystal was mounted on a Rigaku XtaLAB Synergy, Dualflex, HyPix diffractometer. The data collection was performed at 100 K. The structure was solved using Olex2,52 the ShelXT⁵³ structure solution program using the intrinsic phasing method, and refined with the ShelXL⁵⁴ refinement package using least-squares minimization.

Synthetic Procedures. 3,7-Dichloro-5,5-dimethyldibenzo[b,e]silin-10(5H)-one (2). To a flame-dried round-bottom flask under N_2 was added bis(2-bromo-4-chlorophenyl)methane (1, synthesized as previously described, 32 0.891 g, 2.26 mmol) followed by anhydrous THF (10 mL). The reaction was then cooled to -78 °C in a dry ice and acetone bath, and n-BuLi (1.9 mL, 4.75 mmol) was added dropwise over about 5 min. The reaction was allowed to stir for 1 h before adding dichlorodimethylsilane (0.32 mL, 2.7 mmol) dropwise and allowing the reaction to slowly come to room temperature overnight. The next morning, the reaction was quenched with water and extracted with Et2O three times, and the organics were dried over Na₂SO₄ and concentrated via rotary evaporation to an oil. The crude was then passed through a pad of silica using hexanes to yield the intermediate product. The intermediate was transferred to a roundbottom flask, dissolved in acetone (22.0 mL), and purged with N₂ for 10 min before adding KMnO₄ (0.870 g, 5.49 mmol) and allowing the reaction to stir at room temperature. After 20 min, the reaction was passed through a short pad of silica using 100% DCM to yield the crude product. The crude product was then subjected to silica gel chromatography starting with 100% hexanes and gradually increasing to 30% DCM/hexanes to yield the pure product as an off-white solid (0.382 g, 55% overall). 1 H NMR (300 MHz, CDCl₃, Figure S31) δ 8.36 (dd, J = 0.3, 8.0 Hz, 2H), 7.60 (dd, J = 0.3, 2.5 Hz, 2H), 7.54 (dd, 2.2, 8.6 Hz, 2H), 0.52 (s, 6H). ¹³C{¹H} NMR (75 MHz, CDCl₃, Figure S32) δ 168.2, 140.9, 139.3, 138.8, 133.0, 131.2, 130.7, -1.5. HRMS m/z calculated for $C_{15}H_{13}Cl_2OSi [M + H]^+$ 307.0113, found 307.0143. IR (cm⁻¹) 3093, 3074, 3045, 3004, 2959, 2897, 2853, 1922, 1784, 1760, 1644, 1569, 1542, 1492, 1461, 1405, 1370, 1279, 1266, 1242, 1229, 1138, 1102, 1071, 1049.

3,7-Dichloro-5,5-diisopropyldibenzo[b,e]silin-10(5H)-one (3). To a flame-dried round-bottom flask under N_2 was added bis(2-bromo-4chlorophenyl)methane (1, synthesized as previously described,³² 1.98 g, 4.72 mmol) followed by anhydrous THF (200 mL). The reaction was then cooled to -78 °C in a dry ice and acetone bath, and n-BuLi (3.93 mL, 9.43 mmol) was added dropwise over about 10 min. The reaction was allowed to stir for half an hour before adding dichlorodiisopropylsilane (0.93 mL, 5.19 mmol) all at once and allowing the reaction to slowly come to room temperature overnight. The next morning, the reaction was quenched with water and extracted with Et2O three times, and the organics were dried over Na₂SO₄ and concentrated via rotary evaporation to yield a solid. The solids were dissolved in hexanes and passed through a short pad of silica using hexanes to yield the intermediate along with other nonpolar side products. The intermediate was then transferred to a round-bottom flask, dissolved in acetone (22.0 mL), and purged with

N₂ for 10 min before adding KMnO₄ (0.860 g, 5.43 mmol) and allowing the reaction to stir at room temperature. After 20 min, the reaction was passed through a short pad of silica using 100% DCM to yield the crude product. The crude product was then subjected to silica gel chromatography starting with 100% hexanes and gradually increasing to 10% Et₂O/hexanes to yield the pure product as an off-white solid (383 mg, 22%). ¹H NMR (400 MHz, CDCl₃, Figure S33) δ 8.40 (d, J = 8.5 Hz, 2H), 7.61 (d, J = 2.2 Hz, 2H), 7.55 (dd, J = 8.6, 2.2 Hz, 2H), 1.51 (sept, J = 7.4 Hz, 2H), 1.01 (d, J = 7.4 Hz, 12H). 13 C{ 1 H} NMR (101 MHz, CDCl₃, Figure S34) δ 186.4, 140.1, 139.0, 138.0, 133.1, 132.0, 130.6, 17.9, 12.1. HRMS m/z calculated for C₁₉H₂₁Cl₂OSi [M + H]* 363.0739, found 363.0746. IR (cm $^{-1}$) 3055, 2956, 2944, 2925, 2891, 2864, 2836, 1937, 1747, 1648, 1573, 1542, 1460, 1375, 1286, 1270, 1226, 1159, 1137, 1102, 1079.

3,7-Dichloro-5,5-diphenyldibenzo[b,e]silin-10(5H)-one (4). To a flame-dried round-bottom flask under N2 was added bis(2-bromo-4chlorophenyl)methane (1, synthesized as previously described,³² 0.618 g, 1.57 mmol) followed by anhydrous THF (35 mL). The reaction was then cooled to -78 °C in a dry ice and acetone bath, and n-BuLi (1.44 mL, 3.47 mmol) was added dropwise over about 10 min. The reaction was allowed to stir for half an hour before adding dichlorodiphenylsilane (0.40 mL, 1.91 mmol) all at once and allowing the reaction to slowly come to room temperature overnight. The next morning, the reaction was quenched with water and extracted with Et₂O three times, and the organics were dried over Na₂SO₄ and concentrated via rotary evaporation to yield a solid. The solids were dissolved in DCM and passed through a pad of silica using 1:1 DCM/ hexanes to yield the intermediate along with other side products. The intermediate was then transferred to a round-bottom flask, dissolved in acetone (3.0 mL), and purged with N₂ for 10 min before adding KMnO₄ (0.121 g, 0.767 mmol) and allowing the reaction to stir at room temperature. After 20 min, the reaction was passed through a short pad of silica using 100% DCM to yield the crude product. The crude product was then subjected to silica gel chromatography starting with 100% hexanes and gradually increasing to 50% DCM/ hexanes to yield the pure product as an off-white solid (88 mg, 13%). ¹H NMR (400 MHz, CDCl₃, Figure S35) δ 8.41 (d, J = 8.5 Hz, 2H), 7.61-7.56 (ms, 4H), 7.54-7.47 (ms, 6H), 7.40 (t, J = 7.2 Hz, 4H). $^{13}\text{C}\{^{1}\text{H}\}$ NMR (101 MHz, CDCl₃, Figure S36) δ 186.1, 139.7, 139.4, 137.8, 136.1, 134.5, 131.9, 131.3, 131.3, 131.0, 128.7. HRMS m/z calculated for $C_{25}H_{16}Cl_2OSiCs$ [M + Cs]⁺ 562.9402, found 562.9437. IR (cm⁻¹) 3065, 3047, 3015, 3004, 2925, 2853, 1975, 1911, 1897, 1832, 1770, 1742, 1646, 1572, 1542, 1484, 1461, 1428, 1374, 1282, 1271, 1228, 1142, 1103, 1027.

3,7-Dichloro-5,5-bis(2-ethylhexyl)dibenzo[b,e]silin-10(5H)-one (5). The compound was made as previously described.³²

3,7-Dichloro-5,5-bis(3,3,4,4,5,5,6,6,6-nonafluorohexyl)dibenzo-[b,e]silin-10(5H)-one (6). To a flame-dried round-bottom flask under N₂ was added bis(2-bromo-4-chlorophenyl)methane (1, synthesized as previously described,³² 1.00 g, 2.54 mmol) followed by anhydrous THF (51 mL). The reaction was then cooled to −78 °C in a dry ice and acetone bath, and n-BuLi (2.11 mL, 5.07 mmol) was added dropwise over about 10 min. The reaction was allowed to stir for half an hour before adding bis(nonafluorohexyl)dichlorosilane (1.14 mL, 3.05 mmol) dropwise and allowing the reaction to slowly come to room temperature overnight. The next morning, the reaction was quenched with water and extracted with Et₂O three times, and the organics were dried over Na₂SO₄ and concentrated via rotary evaporation to an oil. The oil was dissolved in hexanes and passed through a pad of silica using hexanes to yield the crude intermediate. The intermediate was then added to a flask, dissolved in acetone (6.0 mL), and purged with N₂ for 10 min before adding KMnO₄ (0.243 g, 1.53 mmol) and allowing the reaction to stir at room temperature. After 20 min, the reaction was passed through a short pad of silica using 100% DCM to yield the crude product. The crude product was then subjected to silica gel chromatography starting with 100% hexanes and gradually increasing to 30% DCM/hexanes to yield the pure product as a clear oil (403 mg, 21%). ¹H NMR (300 MHz, CDCl₃, Figure S37) δ 8.46 (d, J = 8.6 Hz, 2H), 7.66 (dd, J = 8.6, 2.2 Hz, 2H), 7.59 (d, I = 2.1 Hz, 2H), 1.95–1.77 (m, 2H), 1.40–1.35 (m,

4H). ${}^{13}C\{{}^{1}H\}$ NMR (101 MHz, CDCl₃, Figure S38) δ 184.9, 140.3, 139.8, 134.6, 132.7, 132.5, 132.2, 122.1, 121.7, 121.4, 120.6, 120.3, 120.0, 119.2, 118.9, 118.5, 118.1, 117.8, 117.5, 116.3, 116.0, 115.7, 115.6, 115.2, 114.9, 113.9, 113.6, 113.5, 113.5, 113.2, 113.1, 112.9, 112.9, 112.8, 112.6, 112.0, 112.0, 111.6, 111.6, 111.2, 111.0, 110.9, 110.6, 110.3, 110.3, 109.9, 109.7, 109.3, 109.3, 109.0, 108.9, 108.6, 108.6, 108.3, 108.3, 108.2, 108.2, 108.0, 107.9, 107.7, 107.6, 106.7, 106.6, 106.3, 105.9, 105.6, 105.5, 105.2, 25.7, 25.4, 25.1, 3.5. Note: The ¹³C NMR for compound 6 contains carbon peaks from 105–122 ppm that originate from the fluoroalkyl groups. Due to the large abundance of fluorine on the alkyl chains, the ¹³C NMR signals exhibit a complex overlapping splitting pattern originating from coupling with the ¹⁹F atoms that results in the appearance of many split carbon signals. All observed signals are reported here. ¹⁹F NMR (400 MHz, CDCl₃, Figure S39) δ -81.05 (t, J = 10.0 Hz), -115.81 (p, J = 15.2 Hz), -123.96 (d, J = 4.2 Hz), -126.13 (q, J = 11.2 Hz).HRMS m/z calculated for $C_{25}H_{15}Cl_2F_{18}OSi~[M + H]^+$ 770.9982, found 770.9986. IR (cm⁻¹) 3048, 2925, 2862, 1650, 1573, 1544, 1460, 1441, 1422, 1376, 1352, 1322, 1288, 1267, 1209, 1167, 1130, 1106, 1069, 1041, 1009.

5,5-Dimethyl-3,7-bis(1-methyl-2-phenylindolizin-3-yl)dibenzo-[b,e]silin-10(5H)-one (7). To a pressure flask in a glovebox with a nitrogen atmosphere were added 3,7-dichloro-5,5-dimethyldibenzo-[b,e] silin-10(5H)-one (2, 503 mg, 1.64 mmol), 1-methyl-2-phenylindolizine (synthesized as previously described, 37 746 mg, 3.60 mmol), Pd(OAc)₂ (37.0 mg, 0.164 mmol), PCy₃HBF₄ (120 mg, 0.327 mmol), and Cs₂CO₃ (3.20 g, 9.82 mmol). The pressure flask was then sealed with a septum and removed from the glovebox. Anhydrous toluene (13.1 mL) was then added, and the pressure flask was sealed and heated to 130 °C using an oil bath. After 52 h, the reaction was cooled to room temperature and passed through a pad of silica starting with 50% DCM/hexanes, followed by 10% acetone/ DCM to elute the pure product as an orange solid (1.06 g, 1.63 mmol, 99% yield). 1 H NMR (400 MHz, CDCl₃, Figure S40) δ 8.48 (d, J=8.3 Hz, 2H), 8.29 (d, J = 7.1 Hz, 2H), 7.73 (d, J = 8.1 Hz, 2H), 7.46 (d, J = 8.8 Hz, 2H), 7.34-7.24 (ms, 12H), 6.77 (t, J = 7.6 Hz, 2H),6.53 (t, J = 6.6 Hz, 2H), 2.40 (s, 6H), 0.03 (s, 6H). $^{13}C\{^{1}H\}$ NMR (101 MHz, CDCl₃, Figure S41) δ 186.9, 139.5, 138.8, 135.5, 135.4, 134.8, 131.6, 130.8, 130.1, 130.0, 129.5, 128.3, 126.6, 122.0, 120.8, 118.0, 117.2, 111.2, 108.3, 9.3, -2.0. HRMS m/z calculated for C₄₅H₃₆N₂OSi [M]⁺ 648.2597, found 648.2617. IR (cm⁻¹) 3051, 2950, 2919, 2861, 1949, 1892, 1757, 1637, 1583, 1538, 1522, 1488, 1446, 1425, 1402, 1378, 1343, 1321, 1288, 1265, 1247, 1159, 1138, 1065, 1034, 1015, 1003.

3,7-Bis(1,2-dimethylindolizin-3-yl)-5,5-dimethyldibenzo[b,e]silin-10(5H)-one (8). To a pressure flask in a glovebox with a nitrogen atmosphere were added 3,7-dichloro-5,5-dimethyldibenzo [b,e] silin-10(5*H*)-one (2, 243 mg, 0.791 mmol), 1,2-dimethylindolizine (synthesized as previously described, 37 253 mg, 1.74 mmol), Pd(OAc)₂ (17.8 mg, 0.0791 mmol), PCy₃HBF₄ (58.3 mg, 0.158 mmol), and Cs₂CO₃ (1.55 g, 4.75 mmol). The pressure flask was then sealed with a septum and removed from the glovebox. Anhydrous toluene (3.2 mL) was then added, and the pressure flask was degassed with N₂ for 20 min before sealing the pressure flask and heating the reaction to 130 °C using an oil bath. After 52 h, the reaction was cooled to room temperature and passed through a short pad of silica using 10% Et₂O/DCM to yield the crude product. The crude product was then purified via silica gel chromatography using 1:1 DCM/ hexanes to yield the pure product as a red solid (228 mg, 0.364 mmol, 46% yield). ¹H NMR (400 MHz, CDCl₃, Figure S42) δ 8.59 (d, J =8.3 Hz, 2H), 8.13 (d, J = 7.2 Hz, 2H), 7.79 (d, J = 1.5 Hz, 2H), 7.71 (dd, J = 1.7, 8.3 Hz, 2H), 7.34 (d, J = 9.0 Hz, 2H), 6.66 (t, J = 7.6 Hz, 2H)2H), 6.41 (t, J = 6.3 Hz, 2H), 2.34 (s, 6H), 2.33 (s, 6H), 0.55 (s, 6H). $^{13}\text{C}\{^{1}\text{H}\}$ NMR (101 MHz, CDCl₃, Figure S43) δ 186.9, 139.6, 139.1, 135.5, 134.0, 131.1, 130.7, 130.4, 123.4, 121.9, 121.0, 117.2, 116.6, 110.2, 108.6, 10.6, 8.8, -1.3. HRMS m/z calculated for $C_{35}H_{32}N_2OSi$ [M]⁺ 524.2284, found 524.2266. IR (cm⁻¹) 3048, 2914, 2857, 2765, 2738, 2656, 1887, 1725, 1638, 1583, 1541, 1506, 1446, 1402, 1382, 1342, 1316, 1286, 1246, 1214, 1153, 1109, 1063, 1022.

5,5-Dimethyl-3,7-bis(1-phenylindolizin-3-yl)dibenzo[b,e]silin-10(5H)-one (9). To a pressure flask in a glovebox with a nitrogen atmosphere were added 3,7-dichloro-5,5-dimethyldibenzo[b,e]silin-10(5H)-one (2, 243 mg, 0.791 mmol), 1-phenylindolizine (synthesized as previously described,³⁶ 336 mg, 1.740 mmol), Pd(OAc)₂ (17.8 mg, 0.0791 mmol), PCy₃HBF₄ (58.3 mg, 0.158 mmol), and Cs₂CO₃ (1.546 g, 4.746 mmol). The pressure flask was then sealed with a septum and removed from the glovebox. Anhydrous toluene (3.2 mL) was then added, and the pressure flask was degassed with N₂ for 20 min before sealing the pressure flask and heating the reaction to 130 °C using an oil bath. After 52 h, the reaction was cooled to room temperature and passed through a short pad of silica using 10% Et₂O/ DCM to yield the crude product. The crude product was then purified via silica gel chromatography using 1:1 DCM/hexanes to yield the pure product as a red solid (228 mg, 0.364 mmol, 46% yield). ¹H NMR (400 MHz, CDCl₃, Figure S44) δ 8.61 (d, J = 8.4 Hz, 2H), 8.43 (d, J = 7.2 Hz, 2H), 7.94 (d, J = 1.8 Hz, 2H), 7.89 (dd, J = 1.9, 8.3 Hz,2H), 7.83 (d, *J* = 9.1 Hz, 2H), 7.67 (dd, *J* = 1.2, 8.3 Hz, 4H), 7.48 (t, *J* = 7.6 Hz, 4H), 7.30 (t, J = 7.4 Hz, 2H), 6.85 (t, J = 8.2 Hz, 2H), 6.63(t, J = 7.4 Hz, 2H), 0.61 (s, 6H). ${}^{13}C\{{}^{1}H\}$ NMR (75 MHz, CDCl₃, Figure S45) δ 186.6, 140.1, 139.3, 135.9, 135.5, 132.3, 131.6, 130.6, 129.0, 128.8, 127.8, 125.9, 124.9, 122.8, 119.2, 119.0, 116.4, 115.1, 112.1, -1.1. HRMS m/z calculated for $C_{43}H_{32}N_2OSi~[M]^+$ 620.2284, found 620.2271. IR (cm⁻¹) 3052, 2951, 2926, 2852, 1637, 1584, 1541, 1510, 1491, 1458, 1440, 1416, 1383, 1359, 1340, 1294, 1247, 1210, 1176, 1150, 1135, 1069, 1031, 1013.

5,5-Diisopropyl-3,7-bis(1-methyl-2-phenylindolizin-3-yl)dibenzo-[b,e]silin-10(5H)-one (10). To a pressure flask in a glovebox with a nitrogen atmosphere were added 3,7-dichloro-5,5-diisopropyldibenzo-[b,e]silin-10(5H)-one (3, 254 mg, 0.702 mmol), 1-methyl-2-phenylindolizine (synthesized as previously described, 37 364 mg, 1.754 mmol), Pd(OAc)₂ (15.8 mg, 0.0702 mmol), PCy₃HBF₄ (51.7 mg, 0.140 mmol), and Cs₂CO₃ (1.37 g, 4.21 mmol). The pressure flask was then sealed with a septum and removed from the glovebox. Anhydrous toluene (5.6 mL) was then added, and the pressure flask was degassed with N2 for 20 min before sealing the pressure flask and heating the reaction to 120 °C using an oil bath. After 24 h, the reaction was cooled to room temperature and purified via silica gel chromatography using 30% DCM/hexanes to yield the pure product as a dark-orange solid (377 mg, 0.535 mmol, 76% yield). ¹H NMR (400 MHz, CDCl₃, Figure S46) δ 8.51 (d, J = 8.3 Hz, 2H), 8.21 (d, J= 7.2 Hz, 2H), 7.74 (dd, J = 1.7, 8.3 Hz, 2H), 7.43 (d, J = 9.0 Hz, 2H), 7.32 (d, J = 1.5 Hz, 2H), 7.30-7.19 (ms, 10H), 6.73 (t, J = 7.7Hz, 2H), 6.49 (t, J = 6.8 Hz, 2H), 2.36 (s, 6H), 0.92 (sept, J = 7.4 Hz, 2H), 0.60 (d, J = 7.4 Hz, 12H). ¹³C{¹H} NMR (101 MHz, CDCl₃, Figure S47) δ 187.4, 140.4, 136.9, 136.0, 135.5, 134.6, 131.4, 130.8, 130.3, 130.1, 129.3, 128.4, 126.5, 122.1, 120.9, 118.0, 117.1, 111.1, 108.3, 17.7, 11.7, 9.4. HRMS m/z calculated for $C_{49}H_{44}N_2OSi$ [M]⁺ 704.3223, found 704.3201. IR (cm⁻¹) 3053, 2940, 2921, 2890, 2861, 1950, 1889, 1756, 1730, 1638, 1584, 1538, 1521, 1489, 1458, 1425, 1404, 1378, 1344, 1321, 1290, 1266, 1240, 1158, 1139, 1067, 1034.

5,5-Diisopropyl-3,7-bis(1-phenylindolizin-3-yl)dibenzo[b,e]silin-10(5H)-one (11). To a pressure flask in a glovebox with a nitrogen atmosphere were added 3,7-dichloro-5,5-diisopropyldibenzo[b,e]silin-10(5H)-one (3, 175 mg, 0.484 mmol), 1-phenylindolizine (synthesized as previously described, ³⁶ 234 mg, 1.21 mmol), Pd(OAc)₂ (10.9 mg, 0.0484 mmol), PCy₃HBF₄ (35.6 mg, 0.0968 mmol), and Cs₂CO₃ (0.946 g, 2.90 mmol). The pressure flask was then sealed with a septum and removed from the glovebox. Anhydrous toluene (3.9 mL) was then added, and the pressure flask was degassed with N2 for 20 min before sealing the pressure flask and heating the reaction to 130 °C using an oil bath. After 30 h, the reaction was cooled to room temperature and passed through a pad of silica gel using 100% DCM to yield the crude product. The crude product was then purified via silica gel chromatography using 50% DCM/hexanes to yield the pure product as a light-orange solid (213 mg, 0.315 mmol, 65% yield). ¹H NMR (300 MHz, CDCl₃, Figure S48) δ 8.64 (d, J = 8.3 Hz, 2H), 8.45 (d, J = 7.2 Hz, 2H), 7.96 (d, J = 1.7 Hz, 2H), 7.90 (dd, J = 1.9, 8.3 Hz,2H), 7.83 (d, J = 9.1 Hz, 2H), 7.68 (d, J = 8.3 Hz, 4H), 7.48 (t, J = 7.8Hz, 4H), 7.31 (t, J = 7.4 Hz, 2H), 7.20 (s, 2H), 6.85 (td, J = 0.6, 9.0

Hz, 2H), 6.64 (td, J = 1.1, 7.3 Hz, 2H), 1.61 (sept, J = 7.4 Hz, 2H), 1.12 (d, J = 7.4 Hz, 12H). ¹³C{¹H} NMR (75 MHz, CDCl₃, Figure S49) δ 187.0, 140.7, 137.0, 136.0, 135.1, 132.4, 131.6, 130.8, 129.0, 128.8, 127.9, 126.0, 125.0, 122.9, 119.1, 119.0, 116.4, 115.1, 112.0, 18.2, 12.3. HRMS m/z calculated for $C_{47}H_{40}N_2OSi [M]^+$ 676.2910, found 676.2937. IR (cm⁻¹) 3051, 2940, 2888, 2861, 1635, 1582, 1540, 1510, 1490, 1459, 1440, 1416, 1382, 1358, 1339, 1290, 1264, 1238, 1208, 1176, 1134, 1069, 1031, 1011.

3,7-Bis(7-(4-(dimethylamino)phenyl)-1-(2-ethylhexyl)-2-phenylindolizin-3-yl)-5,5-diisopropyldibenzo[b,e]silin-10(5H)-one (12). To a pressure flask in a glovebox with a nitrogen atmosphere were added 3,7-dichloro-5,5-diisopropyldibenzo [b,e] silin-10(5H)-one (3, 104 mg, 0.287 mmol), 4-(1-(2-ethylhexyl)-2-phenylindolizin-7-yl)-N,N-dimethylaniline (synthesized as previously described, 18 305 mg, 0.718 mmol), Pd(OAc)₂ (6.4 mg, 0.0287 mmol), PCy₃HBF₄ (21.1 mg, 0.0574 mmol), and Cs_2CO_3 (0.561 g, 1.722 mmol). The pressure flask was then sealed with a septum and removed from the glovebox. Anhydrous toluene (2.3 mL) was then added, and the pressure flask was degassed with N2 for 20 min before sealing the pressure flask and heating the reaction to 130 °C using an oil bath. After 30 h, the reaction was cooled to room temperature and passed through a pad of silica gel using 100% DCM to yield the crude product. The crude product was then purified via silica gel chromatography using 15% EtOAc/hexanes to yield the pure product as a dark-red solid (219 mg, 0.192 mmol, 67% yield). 1 H NMR (400 MHz, CD₂Cl₂, Figure S50) δ 8.43 (d, I = 8.4 Hz, 2H), 8.29 (d, I = 7.4 Hz, 2H), 7.75 (dd, I = 1.5, 8.4 Hz, 2H), 7.60-7.58 (ms, 6H), 7.35 (d, J = 1.3 Hz, 2H), 7.31-7.21 (ms, 10H), 6.84-6.82 (ms, 6H), 3.01 (s, 12H), 2.80-2.69 (m, 4H), 1.42-1.37 (m, 2H), 1.27-1.13 (ms, 16H), 0.96-0.89 (m, 2H), 0.80 (t, J = 6.5 Hz, 6H), 0.72 (t, J = 7.3 Hz, 6H), 0.64 (d, J = 7.2 Hz, 6H)12H). 13 C $\{^{1}$ H $\}$ NMR (101 MHz, CD $_{2}$ Cl $_{2}$, Figure S51) δ 187.1, 140.3, 137.0, 136.5, 136.2, 136.0, 134.9, 134.8, 132.7, 131.2, 130.8, 130.3, 130.1, 130.0, 128.6, 127.5, 126.9, 126.8, 122.6, 113.1, 112.9, 110.5, 41.3, 40.7, 33.1, 29.2, 28.6, 26.2, 23.4, 17.9, 14.3, 12.0, 11.0. HRMS m/z calculated for $C_{79}H_{90}N_4OSi [M]^+$ 1138.6884, found 1138.6846. IR (cm⁻¹) 3053, 2952, 2922, 2857, 2801, 1636, 1608, 1583, 1530, 1483, 1462, 1444, 1420, 1375, 1354, 1290, 1236, 1199, 1160, 1146, 1102, 1066, 1026, 1000

5,5-Bis(2-ethylhexyl)-3,7-bis(1-methyl-2-phenylindolizin-3-yl)dibenzo[b,e]silin-10(5H)-one (13). The compound was made as previously described.³²

3,7-Bis(7-(4-(dimethylamino)phenyl)-1-(2-ethylhexyl)-2-phenylindolizin-3-yl)-5,5-bis(2-ethylhexyl)dibenzo[b,e]silin-10(5H)-one (14). The compound was made as previously described.³²

3,7-Bis(1-methyl-2-phenylindolizin-3-yl)-5,5-bis(3,3,4,4,5,5,6,6,6nonafluorohexyl)dibenzo[b,e]silin-10(5H)-one (15). To a pressure flask in a glovebox were added 3,7-dichloro-5,5-bis(3,3,4,4,5,5,6,6,6nonafluorohexyl)dibenzo[b,e]silin-10(5H)-one (6, 403 mg, 0.519 mmol), 1-methyl-2-phenylindolizine (synthesized as previously described,³⁷ 269 mg, 1.30 mmol), Pd(OAc)₂ (11.7 mg, 0.0519 mmol), PCy₃HBF₄ (38.2 mg, 0.104 mmol), and Cs₂CO₃ (1.02 g, 3.11 mmol). The pressure flask was then sealed with a septum and removed from the glovebox. Anhydrous toluene (4.2 mL) was then added, and the pressure flask was degassed with N2 for 20 min before sealing the pressure flask and heating the reaction to 125 $^{\circ}\text{C}$ using an oil bath. After 21 h, the reaction was cooled to room temperature and passed through a short pad of silica using DCM to yield the crude product. The crude product was then purified via silica gel chromatography using 40% DCM/hexanes to yield the pure product as an orange solid (343 mg, 0.308 mmol, 59% yield). ¹H NMR (400 MHz, CDCl₃, Figure S52) δ 8.52 (d, J = 8.4 Hz, 2H), 8.19 (d, J = 7.2Hz, 2H), 7.75 (d, J = 8.4 Hz, 2H), 7.45 (d, J = 9.0 Hz, 2H), 7.35 (s, 2H), 7.32-7.24 (ms, 6H), 7.21 (d, J = 6.8 Hz, 4H), 6.78 (t, J = 7.7Hz, 2H), 6.51 (t, J = 6.8 Hz, 2H), 2.36 (s, 6H), 1.67 (m, 4H), 0.90 (m, 4H). $^{13}C\{^{1}H\}$ NMR (101 MHz, CDCl₃, Figure S53) δ 185.6, 139.5, 135.9, 135.3, 134.5, 133.3, 131.9, 131.7, 130.9, 130.7, 129.9, 128.4, 127.0, 122.1, 121.8, 121.4, 120.7, 120.4, 120.1, 119.2, 118.9, 118.6, 117.9, 117.6, 116.4, 116.0, 115.7, 115.4, 111.5, 111.0, 110.9, 110.6, 110.3, 110.3, 108.8, 25.5, 25.2, 25.0, 9.3, 3.0. ¹⁹F NMR (400 MHz, CDCl₃, Figure S54) δ -81.03 (t, J = 9.9 Hz), -115.79 (p, J =

15.2 Hz), -123.88 (s), -126.06 (t, J = 14.2 Hz). HRMS m/zcalculated for $C_{55}H_{38}F_{18}N_2OSi\ [M]^+$ 1112.2466, found 1112.2472. IR (cm⁻¹) 3064, 3032, 2921, 2864, 1957, 1889, 1758, 1641, 1584, 1538, 1488, 1445, 1427, 1404, 1379, 1348, 1321, 1290, 1267, 1211, 1161, 1130, 1066, 1037, 1008.

(Z)-3-(5,5-Dimethyl-7-(1-methyl-2-phenylindolizin-3-yl)-10-(otolyl)dibenzo[b,e]silin-3(5H)-ylidene)-1-methyl-2-phenyl-3H-indolizin-4-ium Perchlorate (2Ph-Me). To a flame-dried round-bottom flask under N₂ was added anhydrous THF (2.0 mL) followed by 5,5dimethyl-3,7-bis(1-methyl-2-phenylindolizin-3-yl)dibenzo[*b,e*]silin-10(5H)-one (7, 50 mg, 0.077 mmol). o-Tolylmagnesium bromide (0.19 mL, 0.39 mmol) was then added dropwise to the reaction at room temperature, and the reaction was observed to change colors from orange to dark red almost immediately. After 15 min, the THF was removed under N2 flow followed by vacuum-drying for half an hour. DCM and a couple of drops of water were then added to quench the reaction, which was transferred to a separatory funnel and extracted over 2.0 M $HClO_{4(aq)}$. The solution was observed to rapidly change color from red to dark black. The DCM layer was removed and re-extracted over 2.0 M $HClO_{4(aq)}$. The DCM layer was then passed over a dense plug of glass wool to remove the bulk droplets of the aqueous solution before being concentrated down to \sim 2 mL. The DCM solution was then transferred to centrifuge vials and topped off with Et₂O to precipitate the dye and centrifuged. The supernatant was removed, and the solids were redissolved in minimal DCM, precipitated with Et₂O, and centrifuged again. This process was repeated three times. The solids were then dissolved in DCM and subjected to a cyanosilica column using 50% DCM/hexanes and slowing ramping up to 100% DCM to elute the pure product as a black-colored solution. The black solution was concentrated via rotary evaporation to yield the pure dye as a dark-black solid (21 mg, 0.0240 mmol, 31%). ¹H NMR (300 MHz, CD₂Cl₂, Figure S55) δ 8.63 (d, J =7.1 Hz, 2H), 7.59 (d, J = 8.7 Hz, 2H), 7.53–7.37 (ms, 11H), 7.29– 7.24 (ms, 8H), 7.20–7.14 (ms, 3H) 6.93 (td, J = 0.7, 7.9, 2H), 2.25 (s, 6H), 2.10 (s, 3H), -0.05 (s, 3H), -0.09 (s, 3H). ¹³C{¹H} NMR (101 MHz, CD₂Cl₂, Figure S56) δ 166.7, 145.0, 140.1, 139.8, 138.6, 137.1, 136.9, 136.7, 136.5, 136.3, 134.8, 130.9, 130.6, 129.7, 129.5, 129.3, 128.4, 127.2, 126.6, 126.4, 126.2, 125.9, 119.3, 118.1, 115.7, 19.9, 9.5, -1.7, -2.0. HRMS m/z calculated for $C_{52}H_{43}N_2Si$ [M - ClO_4^{-1} 723.3191, found 723.3168. IR (cm⁻¹) 3056, 2952, 2920, 2859, 1620, 1562, 1522, 1490, 1474, 1445, 1435, 1383, 1318, 1297, 1282, 1207, 1150, 1123, 1090, 1061, 1034, 1009.

(Z)-3-(5,5-Dimethyl-7-(1-phenyl-3H- $4\lambda^4$ -indolizin-3-ylidene)-10-(o-tolyl)-5,7-dihydrodibenzo[b,e]silin-3-yl)-1-phenylindolizine Perchlorate (1Ph-Me). To a flame-dried round-bottom flask under N₂ was added anhydrous THF (2.0 mL) followed by 5,5-dimethyl-3,7bis(1-phenylindolizin-3-yl)dibenzo[b,e]silin-10(5H)-one (8, 50 mg, 0.0805 mmol). o-Tolylmagnesium bromide (0.40 mL, 0.81 mmol) was then added dropwise to the reaction at room temperature, and the reaction was observed to change colors from orange to dark red almost immediately. After 15 min, the THF was removed under N2 flow followed by vacuum-drying for half an hour. DCM and a couple of drops of water were then added to quench the reaction, which was transferred to a separatory funnel and extracted over 2.0 M HClO_{4(aq)}. The solution was observed to rapidly change color from red to dark green. The DCM layer was removed and re-extracted over 2.0 M $HClO_{4(aq)}$. The DCM layer was then passed over a dense plug of glass wool to remove the bulk droplets of the aqueous solution before being concentrated down to ~2 mL. The DCM solution was then transferred to centrifuge vials and topped off with Et₂O to precipitate the dye and centrifuged. The supernatant was removed, and the solids were redissolved in DCM, precipitated with Et₂O, and centrifuged again. This process was repeated three times to yield the pure dye as a dark-magenta-colored solid (29 mg, 0.0362 mmol, 45%). ¹H NMR (400 MHz, CD_2Cl_2 , Figure S57) δ 8.84 (d, J = 6.5 Hz, 2H), 8.19 (s, 2H), 7.96 (d, I = 8.8 Hz, 2H), 7.72-7.66 (ms, 6H), 7.61 (s, 2H), 7.56-7.35 (ms, 13H), 7.25 (d, J = 7.4 Hz, 1H), 7.13 (t, J = 6.7 Hz, 2H), 2.17 (s, 3H), 0.77 (s, 3H), 0.75 (s, 3H). ¹³C{¹H} NMR (101 MHz, CD₂Cl₂, Figure S58) δ 167.6, 146.9, 140.4, 140.1, 138.7, 137.4, 137.3, 136.6, 133.8, 133.4, 131.0, 129.8, 129.7, 129.6, 128.5, 128.2,

128.1, 127.9, 127.7, 126.3, 125.9, 124.7, 121.2, 120.4, 116.7, 19.9, -0.9, -1.1. HRMS m/z calculated for $C_{50}H_{39}N_2Si$ [M - ClO $_4$ $^-$] $^+$ 695.2878, found 695.2869. IR (cm $^{-1}$) 3057, 2958, 2922, 2851, 2641, 2573, 1616, 1563, 1471, 1448, 1433, 1402, 1374, 1339, 1306, 1286, 1244, 1201,1160, 1080, 1027.

(Z)-3-(5,5-Diisopropyl-7-(1-methyl-2-phenylindolizin-3-yl)-10-(otolyl)dibenzo[b,e]silin-3(5H)-ylidene)-1-methyl-2-phenyl-3H-indolizin-4-ium Perchlorate (2Ph-iPr). To a flame-dried round-bottom flask under N2 was added anhydrous THF (5.0 mL) followed by 5,5diisopropyl-3,7-bis(1-methyl-2-phenylindolizin-3-yl)dibenzo[b,e]silin-10(5H)-one (10, 150 mg, 0.213 mmol). o-Tolylmagnesium bromide (0.53 mL, 1.06 mmol) was then added dropwise to the reaction at room temperature, and the reaction was observed to change color from orange to dark red over approximately an hour. After an hour, the THF was removed on a rotary evaporator followed by vacuumdrying for half an hour. DCM and a couple of drops of water were then added to quench the reaction, which was transferred to a separatory funnel and extracted over 2.0 M $\mbox{HClO}_{4(aq)}$. The solution was observed to rapidly change color from red to dark black. The DCM layer was removed and re-extracted over 2.0 M HClO_{4(aq)}. The DCM layer was then passed over a dense plug of glass wool to remove the bulk droplets of the aqueous solution before being concentrated down to \sim 2 mL. Excess Et_2O was then added to precipitate the dye, which was centrifuged, and the supernatant was removed. The crude material was then dissolved in DCM and subjected to silica gel chromatography using 100% DCM and gradually increasing to 20% MeCN/DCM to elute the pure dye as a gray color that when concentrated yielded a sparkly dark-black solid. (76 mg, 0.086 mmol, 41%) ¹H NMR (400 MHz, CD₂Cl₂, Figure S59) δ 8.64 (d, J = 7.0 Hz, 2H), 7.59 (d, J = 8.8 Hz, 2H), 7.51–7.38 (ms, 9H) 7.32 (s, 2H), 7.28-7.24 (ms, 8H), 7.16 (d, J = 7.4 Hz, 1H), 6.93 (t, J = 6.8 Hz, 2H), 2.22 (s, 6H), 2.07 (s, 3H), 0.66-0.60 (ms, 14H). ¹³C{¹H} NMR (101 MHz, CD₂Cl₂, Figure S60) δ 167.2, 142.5, 140.0, 139.8, 138.8, 138.0, 136.9, 136.7, 136.6, 135.9, 134.8, 130.8, 130.4, 129.7, 129.5, 129.4, 128.2, 127.2, 126.6, 126.4, 126.1, 125.9, 119.2, 118.2, 115.6, 19.8, 17.6, 17.4, 13.2, 12.5, 9.4. HRMS m/z calculated for $C_{56}H_{51}N_2Si$ $[M - ClO_4^-]^+$ 779.3817, found 779.3823. IR (cm⁻¹) 3057, 2943, 2922, 2888, 2862, 1619, 1584, 1561, 1521, 1491, 1472, 1444, 1433, 1382, 1344, 1318, 1280, 1203, 1149, 1119, 1090, 1058, 1031.

(Z)-3-(5,5-Diisopropyl-7-(1-phenyl-3H- $4\lambda^4$ -indolizin-3-ylidene)-10-(o-tolyl)-5,7-dihydrodibenzo[b,e]silin-3-yl)-1-phenylindolizine Perchlorate (1Ph-iPr). To a flame-dried round-bottom flask under N₂ was added anhydrous THF (2.0 mL) followed by 5,5-diisopropyl-3,7bis(1-phenylindolizin-3-yl)dibenzo[b,e]silin-10(5H)-one (11, 50 mg, 0.074 mmol). o-Tolylmagnesium bromide (0.19 mL, 0.37 mmol) was then added dropwise to the reaction at room temperature, and the reaction was observed to change color from orange to dark red over approximately half an hour. At this point, the THF was removed on a rotary evaporator followed by vacuum-drying for half an hour. DCM and a couple of drops of water were then added to quench the reaction, which was transferred to a separatory funnel and extracted over 2.0 M HClO_{4(aq)}. The solution was observed to rapidly change color from red to dark black. The DCM layer was removed and reextracted over 2.0 M HClO_{4(aq)}. The DCM layer was then passed over a dense plug of glass wool to remove the bulk droplets of the aqueous solution before being concentrated down to ~2 mL. The crude material was then subjected to silica gel chromatography using 100% DCM and gradually increasing to 20% MeCN/DCM to elute the dye as a greenish-black color that was concentrated to a dark-black solid. The solid was sonicated with Et₂O and centrifuged, and the Et₂O layer was removed 3× to yield the pure dye as a dark-black solid (32 mg, 0.038 mmol, 52%). 1 H NMR (300 MHz, CD₂Cl₂, Figure S61) δ 8.83 (d, J = 7.0 Hz, 2H), 8.17 (d, J = 1.9 Hz, 2H), 7.96 (d, J = 8.9 Hz, 2H), 7.74 (dd, J = 1.8, 9.1 Hz, 2H), 7.66 (d, J = 7.4 Hz, 4H), 7.57-7.36 (ms, 15H), 7.24 (d, J = 7.5 Hz, 1H), 7.12 (td, J = 0.6, 6.9 Hz, 2H), 2.13 (s, 3H), 1.73 (sept, J = 7.6 Hz, 2H), 1.25 (d, J = 7.4 Hz, 6H), 1.19 (d, J = 7.4 Hz, 6H). ¹³C{¹H} NMR (75 MHz, CD₂Cl₂, Figure S62) δ 144.3, 140.9, 140.1, 138.8, 138.5, 137.0, 136.5, 133.8, 133.4, 131.0, 129.8, 129.7, 129.6, 128.4, 128.2, 128.1, 127.7, 127.7, 126.3, 125.9, 124.7, 121.1, 120.4, 116.6, 19.9, 18.2, 18.0, 14.1, 13.5.

HRMS m/z calculated for $C_{54}H_{47}N_2Si~[M~-ClO_4^-]^+$ 751.3504, found 751.3485. IR (cm⁻¹) 3099, 3058, 2946, 2923, 2890, 2862, 1616, 1562, 1469, 1449, 1403, 1374, 1337, 1306, 1286, 1269, 1243, 1199, 1189, 1159, 1071, 1028.

(Z)-7-(4-(Dimethylamino)phenyl)-3-(7-(4-(dimethylamino)phenyl)-1-(2-ethylhexyl)-2-phenylindolizin-3-yl)-5,5-diisopropyl-10-(o-tolyl)dibenzo[b,e]silin-3(5H)-ylidene)-1-(2-ethylhexyl)-2-phenyl-3H-indolizin-4-ium Perchlorate (7DMA-iPr). To a flame-dried round-bottom flask under N₂ were added anhydrous THF (1.1 mL) and 3,7-bis(7-(4-(dimethylamino)phenyl)-1-(2-ethylhexyl)-2-phenylindolizin-3-yl)-5,5-diisopropyldibenzo [b,e] silin-10(5H)-one (12, 50 mg, 0.044 mmol). o-Tolylmagnesium bromide (0.11 mL, 0.22 mmol) was then added dropwise to the reaction at room temperature, and the reaction was observed to change color from red to a brownred over approximately an hour. After an hour, the THF was removed on a rotary evaporator followed by vacuum-drying for half an hour. DCM and a couple of drops of water were then added to quench the reaction, which was transferred to a separatory funnel and extracted over 2.0 M $\text{HClO}_{4(aq)}$. The solution was observed to rapidly change color from light brown-red to dark brown. The DCM layer was removed and re-extracted over 2.0 M $HClO_{4(aq)}$. The DCM layer was then passed over a dense plug of glass wool to remove the bulk droplets of the aqueous solution before being concentrated down to ~2 mL. The DCM solution was then stirred over anhydrous Na₂CO₃ for several hours until the absorption was observed to shift from ~1150 to ~1340 nm, indicating deprotonation of the DMA groups. The Na₂CO₃ was then filtered off, and the DCM layer was concentrated. The crude material was then dissolved in DCM and subjected to silica gel chromatography using 100% DCM and gradually increasing to 20% MeCN/DCM to elute the pure dye as a brown-colored solution that when concentrated vielded a sparkly dark-brown solid. (22 mg, 0.016 mmol, 37%) ¹H NMR (300 MHz, $(CD_3)_2CO$, Figure S63) δ 8.63 (s, 2H), 7.98 (s, 1H), 7.81 (d, J = 8.5Hz, 6H), 7.54-7.45 (ms, 10H), 7.41-7.36 (ms, 10H), 7.20 (d, J = 7.4Hz, 1H), 7.10 (s, 1H), 6.89 (d, J = 8.2 Hz, 4H), 3.08 (s, 12H), 2.78 (s, 3H), 1.45 (m, 2H), 1.26-1.17 (ms, 10H), 1.11 (ms, 10H), 0.78 (t, J = 6.3 Hz, 6H), 0.71-0.68 (ms, 20H). ¹³C(¹H) NMR was not obtained due to insufficient signal and resolution of the dye. HRMS m/z calculated for $C_{86}H_{97}\bar{N}_4Si~[M-ClO_4^-]^+~1213.7478$, found 1213.7528. IR (dispersed in DCM, cm⁻¹) 3380, 3176, 3058, 2954, 2925, 2859, 2803, 2748, 2646, 2547, 1628, 1577, 1561, 1528, 1476, 1436, 1402, 1348, 1329, 1296, 1264, 1223, 1197, 1117, 1080, 1017.

(Z)-3-(5,5-Bis(2-ethylhexyl)-7-(1-methyl-2-phenylindolizin-3-yl)-10-(o-tolyl)dibenzo[b,e]silin-3(5H)-ylidene)-1-methyl-2-phenyl-3Hindolizin-4-ium Perchlorate (2Ph-EtHx). To a flame-dried roundbottom flask under N₂ was added anhydrous THF (5.0 mL) followed by 5,5-bis(2-ethylhexyl)-3,7-bis(1-methyl-2-phenylindolizin-3-yl)dibenzo[b,e]silin-10(5H)-one (13, 150 mg, 0.213 mmol). o-Tolylmagnesium bromide (0.53 mL, 1.06 mmol) was then added dropwise to the reaction at room temperature, and the reaction was observed to change color from orange to dark red over approximately an hour. After an hour, the THF was removed on a rotary evaporator followed by vacuum-drying for half an hour. DCM and a couple of drops of water were then added to quench the reaction, which was transferred to a separatory funnel and extracted over 2.0 M HClO_{4(aq)}. The solution was observed to rapidly change color from red to dark black. The DCM layer was removed and re-extracted over 2.0 M $HClO_{4(ag)}$. The DCM layer was then passed over a dense plug of glass wool to remove the bulk droplets of the aqueous solution before being concentrated down to ~2 mL. To the DCM solution was then added approximately 200 mL of Et₂O, which caused the dye to precipitate as a black solid. The solution was allowed to sit overnight, and the next day, the solids were filtered off, redissolved in DCM, precipitated once more with Et₂O, filtered, and concentrated to yield a shiny dark-black solid. (99 mg, 0.181 mmol, 85%) ¹H NMR (400 MHz, CD₂Cl₂, Figure S64) δ 8.64 (m, 2H), 7.61 (d, J = 8.7 Hz, 2H), 7.50–7.26 (ms, 13H), 7.21-7.16 (ms, 6H), 7.12 (m, 2H), 7.08 (d, J = 7.4, 1H), 6.94 (m, 2H), 2.22 (s, 6H), 2.05 (s, 3H), 1.15-0.83 (ms, 18H), 0.76-0.48 (ms, 16H). $^{13}C\{^{1}H\}$ NMR (101 MHz, CD₂Cl₂, Figure S65) δ 159.2, 140.1, 139.9, 139.8, 139.6, 136.7, 136.1, 136.0, 136.0, 135.9, 135.8,

134.8, 130.8, 129.5, 129.4, 128.4, 127.7, 126.7, 126.6, 126.4, 126.2, 125.8, 119.3, 118.6, 118.5, 118.3, 117.8, 115.7, 115.7, 115.6, 35.6, 35.6, 35.5, 35.4, 29.0, 28.9, 28.8, 28.8, 28.6, 23.3, 23.3, 20.3, 19.8, 14.2, 10.9 10.9, 10.9, 9.4. HRMS m/z calculated for $C_{66}H_{71}N_2Si$ [M - $ClO_4^-]^+$ 919.5382, found 919.5338. IR (cm $^{-1}$) 3055, 2952, 2916, 2852, 1619, 1584, 1561, 1523, 1491, 1473, 1444, 1433, 1381, 1345, 1319, 1281, 1201, 1148, 1119, 1093, 1058, 1029, 1003.

(Z)-7-(4-(Dimethylamino)phenyl)-3-(7-(4-(dimethylamino)phenyl)-1-(2-ethylhexyl)-2-phenylindolizin-3-yl)-5,5-bis(2-ethylhexyl)-10-(o-tolyl)dibenzo[b,e]silin-3(5H)-ylidene)-1-(2-ethylhexyl)-2phenyl-3H-indolizin-4-ium Perchlorate (7DMA-EtHx). To a flamedried round-bottom flask under N2 were added anhydrous THF (0.6 mL) and 3,7-bis(7-(4-(dimethylamino)phenyl)-1-(2-ethylhexyl)-2phenylindolizin-3-yl)-5,5-bis(2-ethylhexyl)dibenzo[*b,e*]silin-10(5*H*)one (14, 30 mg, 0.023 mmol). o-Tolylmagnesium bromide (0.06 mL, 0.12 mmol) was then added dropwise to the reaction at room temperature, and the reaction was observed to change color from red to brown-red over approximately an hour. After an hour, the THF was removed on a rotary evaporator followed by vacuum-drying for half an hour. DCM and a couple of drops of water were then added to quench the reaction, which was transferred to a separatory funnel and extracted over 2.0 M HClO_{4(aq)}. The solution was observed to rapidly change color from light brown-red to dark brown. The DCM layer was removed and re-extracted over 2.0 M $HClO_{4(aq)}$. The DCM layer was then passed over a dense plug of glass wool to remove the bulk droplets of the aqueous solution before being concentrated down to ~2 mL. The DCM solution was then stirred over anhydrous Na₂CO₃ for several hours until the absorption was observed to shift from ~1150 to ~1340 nm, indicating deprotonation of the DMA groups. The Na₂CO₃ was then filtered off, and the DCM layer was concentrated. The crude material was then dissolved in DCM and subjected to silica gel chromatography using 100% DCM and gradually increasing to 20% MeCN/DCM to elute the pure dye as a brown color that when concentrated yielded a sparkly dark-brown solid. (18 mg, 0.012 mmol, 53%) ¹H NMR (300 MHz, (CD₃)₂CO, Figure S66) δ 8.84 (d, J = 8.7 Hz, 2H), 7.99 (s, 2H), 7.81 (d, J = 9 Hz, 4H), 7.63 (s, 2H), 7.56–7.49 (ms, 10H), 7.46–7.36 (ms, 7H), 7.26 (s, 1H), 7.11 (d, J = 6.8 Hz, 1H), 7.02 (s, 1H), 6.89 (d, J = 8.7Hz, 4H), 3.08 (s, 12H), 2.77 (s, 3H), 0.47 (m, 2H), 1.26-1.19 (ms, 12H), 1.11-1.10 (ms, 17H), 1.02 (ms, 13H), 0.78 (t, J = 6.1 Hz, 6H), 0.72-0.69 (ms, 20H). ¹³C{¹H} NMR was not obtained due to insufficient signal and resolution of the dye. HRMS m/z calculated for $C_{96}H_{117}N_4Si~[M-ClO_4^-]^+~1354.9076$, found 1354.9078. IR (dispersed in DCM, cm⁻¹) 3376, 3177, 3057, 2954, 2924, 2855, 2806, 2646, 2540, 1629, 1582, 1565, 1529, 1479, 1439, 1404, 1353, 1299, 1266, 1226, 1200, 1184, 1125, 1091, 1043, 1020, 1000.

(Z)-1-Methyl-3-(7-(1-methyl-2-phenylindolizin-3-yl)-5,5-bis-(3,3,4,4,5,5,6,6,6-nonafluorohexyl)-10-(o-tolyl)dibenzo[b,e]silin-3(5H)-ylidene)-2-phenyl-3H-indolizin-4-ium Perchlorate (2Ph- F_9Hx). To a flame-dried round-bottom flask under N_2 was added anhydrous THF (3.4 mL) followed by 3,7-bis(1-methyl-2-phenylindolizin-3-yl)-5,5-bis(3,3,4,4,5,5,6,6,6-nonafluorohexyl)dibenzo [b,e]silin-10(5H)-one (150 mg, 0.135 mmol). o-Tolylmagnesium bromide (0.34 mL, 0.674 mmol) was then added dropwise to the reaction at room temperature, and the reaction was observed to change color from orange to dark red over about 15 min. Once complete, the THF was removed on a rotary evaporator followed by vacuum-drying for half an hour. DCM and a couple of drops of water were then added to quench the reaction, which was transferred to a separatory funnel and extracted over 2.0 M $\text{HClO}_{4(aq)}$. The solution was observed to rapidly change color from red to dark black. The DCM layer was removed and re-extracted over 2.0 M $HClO_{4(aq)}$. The DCM layer was then passed over a dense plug of glass wool to remove the bulk droplets of the aqueous solution before being concentrated down to ~2 mL. Excess Et₂O was then added to precipitate the dye, which was centrifuged and the supernatant was removed. The crude material was then dissolved in DCM and subjected to silica gel chromatography using 100% DCM and gradually increasing to 20% MeCN/DCM to elute the pure dye as a blue-gray color that when concentrated yielded a sparkly dark-black solid. (39 mg, 0.030 mmol, 22%), ¹H NMR (400

MHz, CD₂Cl₂, Figure S67), δ 8.68 (d, J = 6.9 Hz, 2H), 7.62 (d, J = 8.6 Hz, 4H), 7.50–7.40 (ms, 10H), 7.34 (t, J = 7.6 Hz, 2H), 7.27–7.23 (ms, 7H), 7.12 (d, J = 7.2 Hz, 1H), 7.00 (t, J = 6.9 Hz, 2H), 2.23 (s, 6H), 2.06 (s, 3H), 1.69 (m, 4H), 0.69 (m, 4H). 13 C{ 1 H} NMR (101 MHz, CD₂Cl₂, Figure S68) δ 163.8, 140.7, 139.6, 138.2, 137.2, 136.4, 134.8, 131.0, 130.4, 129.9, 129.7, 129.4, 128.7, 127.7, 127.3, 126.7, 126.4, 120.8, 119.4, 118.6, 118.3, 117.9, 116.7, 116.3, 116.0, 115.7, 111.3, 111.0, 110.6, 109.3, 108.9, 108.6, 25.6, 25.5, 25.4, 25.3, 25.1, 25.0, 19.7, 9.5, 4.1, 3.2. 19 F NMR (400 MHz, CDCl₃, Figure S69) δ -81.3 (q, J = 10.4 Hz), -115.8 (s), -124.0 (s), -124.2 (s), -126.2 (q, J = 8.5 Hz). HRMS m/z calculated for C₆₂H₄₅F₁₈N₂Si [M]⁺ 1187.3060, found 1187.3003. IR (cm⁻¹) 3061, 2924, 2859, 2745, 1620, 1564, 1524, 1476, 1446, 1436, 1352, 1298, 1283, 1207, 1151, 1124, 1061, 1036, 1009.

ASSOCIATED CONTENT

pubs.acs.org/joc

Data Availability Statement

The data underlying this study are available in the published article and its Supporting Information.

Supporting Information

The Supporting Information is available free of charge at https://pubs.acs.org/doi/10.1021/acs.joc.3c01917.

Absorption and emission graphs, CV graphs, computational data table, XYZ coordinates of the optimized dye structures, crystallographic data, stability data, and 1H and $^{13}C\{^1H\}$ NMRs for all new materials synthesized herein (PDF)

Accession Codes

CCDC 2248357 contains the supplementary crystallographic data for this paper. These data can be obtained free of charge via www.ccdc.cam.ac.uk/data_request/cif, or by emailing data_request@ccdc.cam.ac.uk, or by contacting The Cambridge Crystallographic Data Centre, 12 Union Road, Cambridge CB2 1EZ, UK; fax: +44 1223 336033.

AUTHOR INFORMATION

Corresponding Author

Jared H. Delcamp — Department of Chemistry and Biochemistry, University of Mississippi, University, Mississippi 38677, United States; Materials and Manufacturing Directorate (RXNC), Air Force Research Laboratory, Wright-Patterson AFB, Ohio 45433, United States; orcid.org/0000-0001-5313-4078; Email: jared.delcamp.1@us.af.mil.

Authors

William E. Meador – Department of Chemistry and Biochemistry, University of Mississippi, University, Mississippi 38677, United States; Occid.org/0000-0002-9869-026X

Timothy A. Lewis — Department of Chemistry and Biochemistry, University of Mississippi, University, Mississippi 38677, United States; ◎ orcid.org/0009-0009-5222-4819

Abdul K. Shaik – Department of Chemistry and Biochemistry, University of Mississippi, University, Mississippi 38677, United States; orcid.org/0000-0001-9704-9254

Kalpani Hirunika Wijesinghe — Department of Chemistry and Biochemistry, University of Mississippi, University, Mississippi 38677, United States; orcid.org/0000-0002-7049-0370

Boqian Yang — HORIBA Scientific, Piscataway, New Jersey 08854, United States

Amala Dass – Department of Chemistry and Biochemistry, University of Mississippi, University, Mississippi 38677, United States; orcid.org/0000-0001-6942-5451

Nathan I. Hammer – Department of Chemistry and Biochemistry, University of Mississippi, University, Mississippi 38677, United States; Occid.org/0000-0002-6221-2709

Complete contact information is available at: https://pubs.acs.org/10.1021/acs.joc.3c01917

Author Contributions

W.E.M. contributed to the synthesis and characterization of the materials and writing of the manuscript. T.A.L. contributed to the synthesis and characterization of the materials, conducted the stability studies, and assisted in writing of the manuscript. A.K.S. collected and analyzed the fluorescence emission data for the 2Ph and 1Ph derivatives. K.H.W. collected and analyzed the crystallography data. B.Y. collected the fluorescence emission data for the 7DMA derivatives. A.D., N.I.H., and J.H.D. provided intellectual merit, assisted in experimental design, and helped write the manuscript.

Notes

The authors declare the following competing financial interest(s): WEM and JHD have a patent which includes the dyes studied herein.

ACKNOWLEDGMENTS

W.E.M., T.A.L., A.K.S., N.I.H., and J.H.D. thank the National Science Foundation (NSF) for award 1757220 for financial support. K.H.W. and A.D. thank the National Science Foundation for grant CHE-1808138. This material is based on work supported by the National Science Foundation Graduate Research Fellowship Program awarded to W.E.M. Any opinions, findings, and conclusions or recommendations expressed in this material are those of the author(s) and do not necessarily reflect the views of the National Science Foundation. The authors would also like to acknowledge the late Douglas Hamm from HORIBA Scientific for his assistance in facilitating the fluorescence emission data acquisition in this study.

REFERENCES

- (1) Hong, G.; Antaris, A. L.; Dai, H. Near-Infrared Fluorophores for Biomedical Imaging. *Nat. Biomed. Eng.* **2017**, *1*, No. 0010.
- (2) Owens, E. A.; Henary, M.; El Fakhri, G.; Choi, H. S. Tissue-Specific Near-Infrared Fluorescence Imaging. *Acc. Chem. Res.* **2016**, 49, 1731–1740.
- (3) Cosco, E. D.; Arus, B. A.; Spearman, A. L.; Atallah, T. L.; Lim, I.; Leland, O. S.; Caram, J. R.; Bischof, T. S.; Bruns, O. T.; Sletten, E. M. Bright Chromenylium Polymethine Dyes Enable Fast, Four-Color In Vivo Imaging with Shortwave Infrared Detection. *J. Am. Chem. Soc.* **2021**, *143*, 6836–6846.
- (4) Usama, S. M.; Burgess, K. Hows and Whys of Tumor-Seeking Dyes. Acc. Chem. Res. **2021**, *54*, 2121–2131.
- (5) Choi, N. E.; Lee, J. Y.; Park, E. C.; Lee, J. H.; Lee, J. Recent Advances in Organelle-Targeted Fluorescent Probes. *Molecules* **2021**, 26, 217.
- (6) Liu, D.; He, Z.; Zhao, Y.; Yang, Y.; Shi, W.; Li, X.; Ma, H. Xanthene-Based NIR-II Dyes for In Vivo Dynamic Imaging of Blood Circulation. *J. Am. Chem. Soc.* **2021**, *143*, 17136–17143.
- (7) Qi, Y.; Meador, W. E.; Xiong, J.; Abbaszadeh, M.; Thirumala, R. V. K. G.; Delcamp, J. H.; Kundu, S.; Hill, G. A.; Dai, Q. Structural, optical, photocatalytic, and optoelectronic properties of Zn2SnO4 nanocrystals prepared by hydrothermal method. *Nanotechnology* **2021**, *32*, No. 145702.

- (8) Li, Q.; Guo, Y.; Liu, Y. Exploration of Near-Infrared Organic Photodetectors. *Chem. Mater.* **2019**, *31*, 6359–6379.
- (9) Lee, J.; Ko, S.; Lee, H.; Huang, J.; Zhu, Z.; Seifrid, M.; Vollbrecht, J.; Brus, V. V.; Karki, A.; Wang, H.; Cho, K.; Nguyen, T.; Bazan, G. C. Side-Chain Engineering of Nonfullerene Acceptors for Near-Infrared Organic Photodetectors and Photovoltaics. *ACS Energy Lett.* **2019**, *4*, 1401–1409.
- (10) Wang, Y.; Siegmund, B.; Tang, Z.; Ma, Z.; Kublitski, J.; Xing, S.; Nikolis, V. C.; Ullbrich, S.; Li, Y.; Benduhn, J.; Spoltore, D.; Vandewal, K.; Leo, K. Stacked Dual-Wavelength Near-Infrared Organic Photodetectors. *Adv. Opt. Mater.* **2020**, *9* (6), No. 2001784.
- (11) Xue, J.; Li, C.; Xin, L.; Duan, L.; Qiao, J. High-Efficiency and Low Efficiency Roll-Off Near-Infrared Fluorescent OLEDs through Triplet Fusion. *Chem. Sci.* **2016**, *7*, 2888–2895.
- (12) Tuong Ly, K.; Chen-Cheng, R.-W.; Lin, H.-W.; Shiau, Y.-J.; Liu, S.-H.; Chou, P.-T.; Tsao, C.-S.; Huang, Y.-C.; Chi, Y. Near-Infrared Organic Light-Emitting Diodes with Very High External Quantum Efficiency and Radiance. *Nat. Photonics* **2017**, *11*, 63–68.
- (13) Suzuki, H. Organic Light-Emitting Materials and Devices for Optical Communication Technology. *J. Photochem. Photobiol., A* **2004**, *166*, 155–161.
- (14) Carr, J. A.; Aellen, M.; Franke, D.; So, P. T. C.; Bruns, O. T.; Bawendi, M. G. Absorption by water increases fluorescence image contrast of biological tissue in the shortwave infrared. *Proc. Natl. Acad. Sci. U.S.A.* 2018, 115, 9080.
- (15) Wang, S.; Fan, Y.; Li, D.; Sun, C.; Lei, Z.; Lu, L.; Wang, T.; Zhang, F. Anti-quenching NIR-II molecular fluorophores for in vivo high-contrast imaging and pH sensing. *Nat. Commun.* **2019**, *10*, No. 1058.
- (16) Yang, Y.; Sun, C.; Wang, S.; Yan, K.; Zhao, M.; Wu, B.; Zhang, F. Counterion-Paired Bright Heptamethine Fluorophores with NIR-II Excitation and Emission Enable Multiplexed Biomedical Imaging. *Angew. Chem., Int. Ed.* **2022**, *61* (24), No. e202117436.
- (17) Ding, B.; Xiao, Y.; Zhou, H.; Zhang, X.; Qu, C.; Xu, F.; Deng, Z.; Cheng, Z.; Hong, X. Polymethine Thiopyrylium Fluorophores with Absorption beyond 1000 nm for Biological Imaging in the Second Near-Infrared Subwindow. J. Med. Chem. 2019, 62, 2049–2059
- (18) Ndaleh, D.; Smith, C.; Loku Yaddehige, M.; Shaik, A. K.; Watkins, D. L.; Hammer, N. I.; Delcamp, J. H. Shortwave Infrared Absorptive and Emissive Pentamethine-Bridged Indolizine Cyanine Dyes. J. Org. Chem. 2021, 86, 15376–15386.
- (19) Cosco, E. D.; Spearman, A. L.; Ramakrishnan, S.; Lingg, J. G. P.; Saccomano, M.; Pengshung, M.; Arus, B. A.; Wong, K. C. Y.; Glasl, S.; Ntziachristos, V.; Warmer, M.; McLaughlin, R. R.; Bruns, O. T.; Sletten, E. M. Shortwave infrared polymethine fluorophores matched to excitation lasers enable non-invasive, multicolour in vivo imaging in real time. *Nat. Chem.* **2020**, *12*, 1123–1130.
- (20) Li, B.; Lu, L.; Zhao, M.; Lei, Z.; Zhang, F. An Efficient 1064 nm NIR-II Excitation Fluorescent Molecular Dye for Deep-Tissue High-Resolution Dynamic Bioimaging. *Angew. Chem., Int. Ed.* **2018**, *57*, 7483–7487.
- (21) Liu, M. H.; Zhang, Z.; Yang, Y. C.; Chan, Y. H. Polymethine-Based Semiconducting Polymer Dots with Narrow-Band Emission and Absorption/Emission Maxima at NIR-II for Bioimaging. *Angew. Chem., Int. Ed.* **2021**, *60*, 983–989.
- (22) Dou, K.; Feng, W.; Fan, C.; Cao, Y.; Xiang, Y.; Liu, Z. Flexible Designing Strategy to Construct Activatable NIR-II Fluorescent Probes with Emission Maxima beyond 1200 nm. *Anal. Chem.* **2021**, 93, 4006–4014.
- (23) Bai, L.; Sun, P.; Liu, Y.; Zhang, H.; Hu, W.; Zhang, W.; Liu, Z.; Fan, Q.; Li, L.; Huang, W. Novel aza-BODIPY based small molecular NIR-II fluorophores for in vivo imaging. *Chem. Commun.* **2019**, *55*, 10920–10923.
- (24) Wang, Y.; Wang, M.; Xia, G.; Yang, Y.; Si, L.; Wang, H.; Wang, H. Maximal Emission beyond 1200 nm Dicyanovinyl-Functionalized Squaraine for in vivo Vascular Imaging. *Chem. Commun.* **2023**, *59*, 3598.

- (25) Antaris, A. L.; Chen, H.; Cheng, K.; Sun, Y.; Hong, G.; Qu, C.; Diao, S.; Deng, Z.; Hu, X.; Zhang, B.; Zhang, X.; Yaghi, O. K.; Alamparambil, Z. R.; Hong, X.; Cheng, Z.; Dai, H. A Small-Molecule Dye for NIR-II Imaging. *Nat. Mater.* **2016**, *15*, 235–242.
- (26) Fang, Y.; Shang, J.; Liu, D.; Shi, W.; Li, X.; Ma, H. Design, Synthesis, and Application of a Small Molecular NIR-II Fluorophore with Maximal Emission beyond 1200 nm. *J. Am. Chem. Soc.* **2020**, 142, 15271–15275.
- (27) Antaris, A. L.; Chen, H.; Diao, S.; Ma, Z.; Zhang, Z.; Zhu, S.; Wang, J.; Lozano, A. X.; Fan, Q.; Chew, L.; Zhu, M.; Cheng, K.; Hong, X.; Dai, H.; Cheng, Z. A High Quantum Yield Molecule-Protein Complex Fluorophore for Near-Infrared II Imaging. *Nat. Commun.* 2017, 8, No. 15269.
- (28) Chatterjee, S.; Shaik, A. K.; Wijesinghe, K. H.; Ndaleh, D.; Dass, A.; Hammer, N. I.; Delcamp, J. H. Design and Synthesis of RhodIndolizine Dyes with Improved Stability and Shortwave Infrared Emission up to 1250 nm. *J. Org. Chem.* 2022, 87, 11319.
- (29) Rathnamalala, C. S. L.; Gayton, J. N.; Dorris, A. L.; Autry, S. A.; Meador, W.; Hammer, N. I.; Delcamp, J. H.; Scott, C. N. Donor-Acceptor-Donor NIR II Emissive Rhodindolizine Dye Synthesized by C-H Bond Functionalization. *J. Org. Chem.* **2019**, *84*, 13186–13193.
- (30) Grzybowski, M.; Morawski, O.; Nowak, K.; Garbacz, P. Fluorene analogues of xanthenes low molecular weight near-infrared dyes. *Chem. Commun.* **2022**, *58*, 5455–5458.
- (31) Chatterjee, S.; Meador, W. E.; Smith, C.; Chandrasiri, I.; Zia, M. F.; Nguyen, J.; Dorris, A. L.; Flynt, A. S.; Watkins, D. L.; Hammer, N. I.; Delcamp, J. H. SWIR emissive RosIndolizine dyes with nanoencapsulation in water soluble dendrimers. *RSC Adv.* **2021**, *11*, 27832–27836.
- (32) Meador, W. E.; Lin, E. Y.; Lim, I.; Friedman, H. C.; Ndaleh, D.; Shaik, A. K.; Hammer, N. I.; Yang, B.; Caram, J. R.; Sletten, E. M.; Delcamp, J. H., Shortwave Infrared Absorbing and Emitting Silicon-Rosindolizine Fluorophores for in vivo Fluorescence Imaging. *Nat. Chem.* **2023**, DOI: 10.1038/s41557-024-01464-6.
- (33) Lei, Z.; Li, X.; Li, Y.; Luo, X.; Zhou, M.; Yang, Y. Synthesis of Sterically Protected Xanthene Dyes with Bulky Groups at C-3' and C-7'. J. Org. Chem. 2015, 80, 11538–11543.
- (34) Takeyama, Y.; Oshima, K.; Utimoto, K. Base Induced Reaction of Silacyclobutane with Aldehyde or Epoxide. *Tetrahedron Lett.* **1990**, 31, 6059–6062.
- (35) Sheikh, M. R. K.; Imae, I.; Tharanikkarasu, K.; LeStrat, V. M.; Kawakami, Y. Silacyclobutanes as "Carbanion Pump" in anionic Polymerization I. Anionic Polymerization of Styrene by Potassium t-Butoxide in the Presence of Silacyclobutanes. *Polym. J.* **2000**, 32, 527–530.
- (36) Pohjala, E. A Facile Synthesis of Stable Dihydroindolizines via Intramolecular 1,5-Cyclization of Ylides. *Tetrahedron Lett.* **1972**, *13*, 2585–2588.
- (37) McNamara, L. E.; Rill, T. A.; Huckaba, A. J.; Ganeshraj, V.; Gayton, J.; Nelson, R. A.; Sharpe, E. A.; Dass, A.; Hammer, N. I.; Delcamp, J. H. Indolizine-Squaraines: NIR Fluorescent Materials with Molecularly Engineered Stokes Shifts. *Chem. Eur. J.* **2017**, 23, 12494—12501.
- (38) Frisch, M. J.; Pople, J. A.; Binkley, J. S. Self-consistent molecular orbital methods 25. Supplementary functions for Gaussian basis sets. *J. Chem. Phys.* **1984**, *80*, 3265–3269.
- (39) Lee, C.; Yang, W.; Parr, R. G. Development of the Colle-Salvetti correlation-energy formula into a functional of the electron density. *Phys. Rev. B* **1988**, *37*, 785–789.
- (40) Becke, A. D. Density-functional thermochemistry. III. The role of exact exchange. *J. Chem. Phys.* **1993**, *98*, 5648–5652.
- (41) Frisch, M. J.; Trucks, G. W.; Schlegel, H. B.; Scuseria, G. E.; Robb, M. A.; Cheeseman, J. R.; Scalmani, G.; Barone, V.; Petersson, G. A.; Nakatsuji, H.; Li, X.; Caricato, M.; Marenich, A. V.; Bloino, J.; Janesko, B. G.; Gomperts, R.; Mennucci, B.; Hratchian, H. P.; Ortiz, J. V.; Izmaylov, A. F.; Sonnenberg, J. L.; Williams-Young, D.; Ding, F.; Lipparini, F.; Egidi, F.; Goings, J.; Peng, B.; Petrone, A.; Henderson, T.; Ranasinghe, D.; Zakrzewski, V. G.; Gao, J.; Rega, N.; Zheng, G.; Liang, W.; Hada, M.; Ehara, M.; Toyota, K.; Fukuda, R.; Hasegawa, J.;

- Ishida, M.; Nakajima, T.; Honda, Y.; Kitao, O.; Nakai, H.; Vreven, T.; Throssell, K.; Montgomery, J. A., Jr.; Peralta, J. E.; Ogliaro, F.; Bearpark, M. J.; Heyd, J. J.; Brothers, E. N.; Kudin, K. N.; Staroverov, V. N.; Keith, T. A.; Kobayashi, R.; Normand, J.; Raghavachari, K.; Rendell, A. P.; Burant, J. C.; Iyengar, S. S.; Tomasi, J.; Cossi, M.; Millam, J. M.; Klene, M.; Adamo, C.; Cammi, R.; Ochterski, J. W.; Martin, R. L.; Morokuma, K.; Farkas, O.; Foresman, J. B.; Fox, D. J. *Gaussian 16*, Revision A.03; Gaussian, Inc.: Wallingford CT, 2016.
- (42) Gayton, J.; Autry, S. A.; Meador, W.; Parkin, S. R.; Hill, G. A.; Hammer, N. I.; Delcamp, J. H. Indolizine-Cyanine Dyes: Near Infrared Emissive Cyanine Dyes with Increased Stokes Shifts. *J. Org. Chem.* **2019**, *84*, 687–697.
- (43) Cosco, E. D.; Caram, J. R.; Bruns, O. T.; Franke, D.; Day, R. A.; Farr, E. P.; Bawendi, M. G.; Sletten, E. M. Flavylium Polymethine Fluorophores for Near- and Shortwave Infrared Imaging. *Angew. Chem., Int. Ed.* **2017**, *56*, 13126–13129.
- (44) Elgrishi, N.; Rountree, K. J.; McCarthy, B. D.; Rountree, E. S.; Eisenhart, T. T.; Dempsey, J. L. A Practical Beginner's Guide to Cyclic Voltammetry. *J. Chem. Educ.* **2018**, *95*, 197.
- (45) Frisch, M. J.; Trucks, G. W.; Schlegel, H. B.; Scuseria, G. E.; Robb, M. A.; Cheeseman, J. R.; Scalmani, G.; Barone, V.; Petersson, G. A.; Nakatsuji, H.; Li, X.; Caricato, M.; Marenich, A. V.; Bloino, J.; Janesko, B. G.; Gomperts, R.; Mennucci, B.; Hratchian, H. P.; Ortiz, J. V.; Izmaylov, A. F.; Sonnenberg, J. L.; Williams; Ding, F.; Lipparini, F.; Egidi, F.; Goings, J.; Peng, B.; Petrone, A.; Henderson, T.; Ranasinghe, D.; Zakrzewski, V. G.; Gao, J.; Rega, N.; Zheng, G.; Liang, W.; Hada, M.; Ehara, M.; Toyota, K.; Fukuda, R.; Hasegawa, J.; Ishida, M.; Nakajima, T.; Honda, Y.; Kitao, O.; Nakai, H.; Vreven, T.; Throssell, K.; Montgomery, J. A., Jr.; Peralta, J. E.; Ogliaro, F.; Bearpark, M. J.; Heyd, J. J.; Brothers, E. N.; Kudin, K. N.; Staroverov, V. N.; Keith, T. A.; Kobayashi, R.; Normand, J.; Raghavachari, K.; Rendell, A. P.; Burant, J. C.; Iyengar, S. S.; Tomasi, J.; Cossi, M.; Millam, J. M.; Klene, M.; Adamo, C.; Cammi, R.; Ochterski, J. W.; Martin, R. L.; Morokuma, K.; Farkas, O.; Foresman, J. B.; Fox, D. J. Gaussian 16, Rev. C.01; Gaussian, Inc.: Wallingford, CT, 2016.
- (46) Lee, C.; Yang, W.; Parr, R. G. Development of the Colle-Salvetti correlation-energy formula into a functional of the electron density. *Phys. Rev. B: Condens. Matter* **1988**, *37*, 785–789.
- (47) Francl, M. M.; Pietro, W. J.; Hehre, W. J.; Binkley, J. S.; Gordon, M. S.; DeFrees, D. J.; Pople, J. A. Self-consistent molecular orbital methods. XXIII. A polarization-type basis set for second-row elements. *J. Chem. Phys.* 1982, 77, 3654–3665.
- (48) Hehre, W. J.; Ditchfield, R.; Pople, J. A. Self-Consistent Molecular Orbital Methods. XII. Further Extensions of Gaussian-Type Basis Sets for Use in Molecular Orbital Studies of Organic Molecules. *J. Chem. Phys.* **1972**, *56*, 2257–2261.
- (49) Miertus, S.; Scrocco, E.; Tomasi, J. Electrostatic Interaction of a Solute with a Continuum. A Direct Utilization of AB Initio Molecular Potentials for the Prevision of Solvent Effects. *Chem. Phys.* **1981**, *55*, 117–129.
- (50) Miertus, S.; Tomasi, J. Approximate Evaluations of the Electrostatic Free Energy and Internal Energy Changes in Solution Processes. *Chem. Phys.* **1982**, *65*, 239–245.
- (51) Pascual-Ahuir, J. L.; Silla, E.; Tunon, I. GEPOL: An Improved Description of Molecular Surfaces. III. A New Algorithm for the Computation of a Solvent-Excluding Surface. *J. Comput. Chem.* **1994**, *15*, 1127–1138.
- (52) Dolomanov, O. V.; Bourhis, L. J.; Gildea, R. J.; Howard, J. A.; Puschmann, H. OLEX2: A Complete Structure Solution, Refinement and Analysis Program. *J. Appl. Crystallogr.* **2009**, *42*, 339–341.
- (53) Sheldrick, G. M. SHELXT—Integrated Space-Group and Crystal-Structure Determination. *Acta Crystallogr., Sect. A: Found. Adv.* **2015**, *71*, 3–8.
- (54) Sheldrick, G. M. Crystal Structure Refinement with SHELXL. Acta Crystallogr., Sect. C: Struct. Chem. 2015, 71, 3-8.